

NACA RM No. L8F21

22 JUL 1948

~~CONFIDENTIAL~~



# RESEARCH MEMORANDUM

DOWNWASH AND DYNAMIC PRESSURE AT THE HORIZONTAL  
TAIL OF A SIX-ENGINE PUSHER-PROPELLED AIRPLANE

By

G. Chester Furlong

Langley Aeronautical Laboratory  
Langley Field, Va.

CLASSIFICATION CANCELLED

CLASSIFICATION CHANGED

Authority NACA R 7 2388 Date 8/18/54

CLASSIFIED DOCUMENT

~~CONFIDENTIAL~~

By WTA 8/31/54 See

To  
This document contains classified information affecting the National Defense of the United States within the meaning of the Espionage Act, Title 18, U.S.C. Sec. 793 and 794. Its transmission or the revelation of its contents in any manner to an unauthorized person is prohibited by law. Information so classified may be imparted only to persons in the military or naval service of the United States, to the civilian officers and employees of the Federal Government who have a legitimate interest therein, and to United States citizens of known loyalty and discretion who of necessity must be informed thereof.

Interim copy date 12/11/53  
Proc R 7 1782 E 8 10581

## NATIONAL ADVISORY COMMITTEE FOR AERONAUTICS

WASHINGTON  
July 19, 1948

~~CONFIDENTIAL~~

NACA LIBRARY

LANGLEY MEMORIAL AERONAUTICAL  
LABORATORY  
Langley Field, Va.

RESTRICTED

UNCLASSIFIED

UNCLASSIFIED

NACA RM No. L8F21

~~RESTRICTED~~

~~CONFIDENTIAL~~

NATIONAL ADVISORY COMMITTEE FOR AERONAUTICS

---

RESEARCH MEMORANDUM

---

DOWNWASH AND DYNAMIC PRESSURE AT THE HORIZONTAL  
TAIL OF A SIX-ENGINE PUSHER-PROPELLED AIRPLANE

By G. Chester Furlong

SUMMARY

Air-stream surveys have been made in the vertical plane of the elevator hinge line of a powered model of a high-wing, six-engine, heavy, pusher-propelled bomber. The values of downwash and dynamic-pressure ratio obtained from the air-stream surveys are presented in the form of contour charts.

Average values of downwash and dynamic-pressure ratio obtained from air-stream-survey data are compared with effective values obtained from force and moment data. The comparison was made to investigate means of employing air-stream surveys to estimate the contribution of the tail to the stability of the airplane.

The results of the tests indicated that the average values of downwash obtained from air-stream surveys were approximately  $1^{\circ}$  to  $2^{\circ}$  greater than the effective values obtained from force and moment data. A concept that the part of the tail intercepted by the fuselage contributed little, if any, to the evaluation of the effective values of downwash angle from force and moment data was used to obtain an empirical formula by which average values of downwash angle obtained from air-stream surveys could be made to agree satisfactorily with effective values. The average values of dynamic-pressure ratio obtained by the use of the empirical method did not agree satisfactorily with the effective values of dynamic-pressure ratio obtained from force and moment data. The disagreement was attributed to the accuracy with which effective values of dynamic-pressure ratio could be obtained from force and moment data.

For all flap conditions (retracted and deflected) the tail passed into the center of the wake at moderate to high angles of attack. The nacelle-wing juncture, the fuselage-wing juncture, and the nacelle had a pronounced effect on the flow at the tail. There was no severe distortion of the slipstream. When the flaps were deflected, the effects of the upgoing and downgoing blades were not reversed as previously reported for a tractor airplane.

UNCLASSIFIED

~~CONFIDENTIAL~~

~~RESTRICTED~~

## INTRODUCTION

Air-stream surveys made in the region of a horizontal tail are useful, at present, to study the effects of slipstream and fuselage interference. In order to complete the usefulness of air-stream surveys, it should be possible to obtain average values of downwash and dynamic pressure for use in the estimation of the contribution of the tail to the longitudinal stability of an airplane. The average values obtained from air-stream surveys for most normal tail locations, however, do not agree with effective values determined from force and moment data. These discrepancies probably arise from the inexactness of the method used to compute the lift of a tail that is operating in the field of fuselage interference and varying dynamic pressure.

Some insight into the discrepancies between average and effective values and the general interference problem was obtained during the wind-tunnel investigation in the Langley 19-foot pressure tunnel of a  $\frac{1}{14}$ -scale powered model of a high-wing, six-engine, heavy, pusher-propelled bomber. Air-stream surveys, obtained to study the air flow behind a pusher-propelled airplane, were made in the vertical plane of the elevator hinge line; and these data in conjunction with force and moment data of the complete model provide a comparison of average values of downwash and dynamic-pressure ratio obtained from air-stream surveys with effective values obtained from tail-on and tail-off force and moment data.

The present paper contains the air-stream surveys presented as contour charts of dynamic-pressure ratio and downwash obtained in the vertical plane of the elevator hinge line of the pusher-propelled airplane. Average and effective values of downwash and dynamic-pressure ratio are compared. An empirical equation is presented which brings average values of downwash into agreement with effective values.

## SYMBOLS

$C_L$  lift coefficient ( $L/qS$ )

$C_m$  pitching-moment coefficient ( $M/qS\bar{c}$ )

$C_{L\alpha_t}$  slope of tail lift curve  $\left( \left[ \left( \frac{dC_L}{d\alpha} \right)_t = - \frac{(C_{m_{1t}})_0}{\frac{S_t}{S} \frac{l}{c}} \right]_{\frac{q_t}{q} = 1.00} \right)$

$C_{m_t}$  pitching-moment coefficient contributed by tail

$C_{m_{1t}}$	effectiveness of stabilizer $\left(\frac{dC_m}{di_t}\right)$
A	aspect ratio $\left(b^2/S\right)$
$a_0$	two-dimensional lift-curve slope $\left(\frac{dc_l}{d\alpha_0}\right)$
$q_t/q$	ratio of dynamic pressure at tail to free-stream dynamic pressure
$\epsilon$	angle of downwash, degrees
L	lift, pounds
M	pitching moment, pound-feet
q	dynamic pressure, pounds per square foot $\left(\frac{1}{2}\rho V^2\right)$
S	surface area, square feet
$\bar{c}$	mean aerodynamic chord (M.A.C.), feet
c	local chord, feet
b	surface span, feet
y	spanwise station, feet
l	tail length, distance from 0.25 M.A.C. of wing to 0.25 M.A.C. of tail
$\alpha$	angle of attack, degrees
$i_t$	stabilizer incidence with respect to wing root chord, degrees
$\delta_f$	flap deflection, degrees
$\alpha_0$	section angle of attack in two-dimensional flow, degrees
$c_l$	section lift coefficient
R	Reynolds number $\left(\rho V \bar{c} / \mu\right)$
$\rho$	mass density of air, slugs per cubic foot
$\mu$	coefficient of viscosity of air, slugs per foot-second
V	velocity of air, feet per second
$T_c$	thrust disk-loading coefficient $\left(\frac{T - \Delta D}{2qD^3}\right)$
$Q_c$	torque disk-loading coefficient $\left(Q/2qD^3\right)$
$\Delta D$	change in airplane drag due to slipstream and inflow effects of propeller, pounds

D diameter of propeller, feet  
 T propeller thrust, pounds  
 Q propeller torque, pound-feet  
 $\beta$  propeller blade angle measured at 0.75 radius, degrees  
 $2y/b$  spanwise distance

Subscripts:

o free-stream  
 w wing  
 t tail  
 iso isolated tail  
 av average weighted values obtained from air-stream surveys  
 eff effective values obtained from force and moment data

Primes indicate average values obtained from air-stream surveys using an effective span.

## MODEL, APPARATUS, AND TESTS

### Model

The design characteristics, pertinent to the present tests, of the  $\frac{1}{14}$ -scale powered model of a high-wing, six-engine, heavy, pusher-propelled bomber are given in table I. A three-view drawing of the model is presented as figure 1. The model set up for the air-stream surveys in the Langley 19-foot pressure tunnel is shown as figure 2.

The circular fuselage was equipped with protuberances such as navigator's dome, mast antennas, sighting-station "blisters," and radar fairings. The tail radar fairing was constructed as an integral part of the tail assembly. A drawing of the horizontal tail is presented as figure 3.

The wing contained midchord slots in the wing outer panels ahead of the ailerons. Six partly submerged nacelles extended from the trailing edge. The single slotted flaps extended from the fuselage to the outboard nacelles and were interrupted by both inboard and both center nacelles.

When the flaps were deflected, the landing gear was extended and the mid-chord slots were open. The wells for the main wheels were exposed when the landing gear was extended and were covered with fairings when the gear was retracted. No fillets were used at the fuselage-wing or the nacelle-wing junctures.

The model was equipped with six, three-blade, left-hand, pusher propellers that were geometrically similar to the Curtiss No. 1129-IC6-24 propeller. Each propeller was driven by a water-cooled, alternating-current induction motor housed in the wing. The power delivered to the motors was determined from a calibration involving motor torque, current, and rotational speed.

The surface of the model was maintained in a smooth condition.

### Survey Apparatus

The air-stream survey rake for the Langley 19-foot pressure tunnel (fig. 4) was used to obtain dynamic pressures and downwash. The rake consists of six pitot-static tubes with pitch and yaw orifices (two each) drilled in the hemispherical tips at  $45^\circ$  to the longitudinal tube axes and at  $90^\circ$  to each other. The tubes are alined in a vertical plane and are spaced 3 inches. The pitch (downwash), yaw (sidewash), and dynamic-pressure orifices had been previously calibrated through a known pitch and yaw range.

All pressure leads were conducted from the air-stream survey rake (fig. 4) through the survey strut and from there to a multiple-tube manometer. The manometer readings were photographically recorded during the tests.

The mechanism of the survey-strut carriage allowed the rake to traverse a plane perpendicular to the longitudinal tunnel axis.

### Tests

The air-stream-survey tests and the force and moment tests were made with the density of the atmosphere in the tunnel maintained at approximately 0.00545 slug per cubic foot and the dynamic pressure maintained at 25 pounds per square foot. These conditions correspond to a Reynolds number of approximately 2,400,000 based on the M.A.C. of the wing. The model was tested with the flaps retracted, the flaps deflected  $20^\circ$  (take-off condition), and the flaps deflected  $40^\circ$  (landing condition).

The power conditions for the model tests simulated the full-scale power conditions given in table II. The model propellers were operated to obtain exactly the calculated values of thrust coefficient for given

values of lift coefficient (fig. 5) and to approximate the torque coefficients at corresponding thrust coefficients (fig. 6) for the full-scale airplane. A blade angle of  $21^\circ$  was found to approximate satisfactorily the desired torque.

The air-stream survey rake was set at 12 spanwise locations for each angle of attack (as shown in fig. 7) along a line corresponding to the approximate location of the elevator hinge line. Two vertical settings of the rake were made at each spanwise location so that measurements were spaced 1.5 inches. Because it was not practical to change the longitudinal location of the survey apparatus during the tests, a location was selected so that the forward and rearward movement of the elevator hinge line varied no more than 0.5 inch from the longitudinal plane for the angles of attack tested.

## RESULTS AND DISCUSSION

### Reduction of Data

The original air-stream-survey data have been cross-plotted to obtain contour charts of dynamic-pressure ratio and downwash in the vertical plane of the elevator hinge line. The tail-off lift curves together with the contour charts are presented in figures 8 to 15. Table III summarizes the contour charts presented. The jet-boundary corrections applied to the data consist of an angle change to the downwash and a downward displacement to the field of flow. The wing angles of attack have been corrected for jet-boundary effects and stream-angle misalignment.

Table IV contains average weighted values of dynamic-pressure ratio and downwash for all conditions tested. They were obtained by weighting the local values measured along the hinge line according to the following equations:

$$\left(\frac{q_t}{q}\right)_{av} = \frac{1}{S_t} \int_{-\frac{b_t}{2}}^{\frac{b_t}{2}} \frac{q_t}{q} c_t db_t$$

and

$$\epsilon_{av} = \frac{1}{S_t \left(\frac{q_t}{q}\right)_{av}} \int_{-\frac{b_t}{2}}^{\frac{b_t}{2}} \frac{q_t}{q} \epsilon c_t db_t \quad (1)$$

Faired values of  $q_t/q$  and  $\epsilon$  were used over the part of the span covered by the fuselage.

The effective values of downwash and dynamic-pressure ratio have been computed for the same model and power conditions as were the air-stream surveys. These values are included in table IV. The computations are based on tail-on and tail-off force and moment data. Representative force and moment data are presented in figure 16 for  $\delta_F = 0^\circ$  and rated power. The data presented have been corrected for jet-boundary effects and model-support tare. Because isolated-tail tests showed a constant lift-curve slope through the angle-of-attack range of the tail on the model, the computations were simplified to

$$\left(\frac{q_t}{q}\right)_{\text{eff}} = \frac{C_{m_{1t}}}{(C_{m_{1t}})_0}$$

and

$$\alpha_t = \frac{C_{m_t}}{C_{m_{1t}}}$$

which makes

$$\epsilon_{\text{eff}} = \alpha_w + i_t - \alpha_t$$

The value of  $(C_{m_{1t}})_0$  was obtained from tail-on tests at  $C_{L_w} = 0$ . The assumption that this value corresponds to  $\frac{q_t}{q} = 1.00$  is usually justified within 2 or 3 percent. The computed values of  $\epsilon_{\text{eff}}$  have been corrected for jet-boundary effects.

#### Air-Stream Surveys

Downwash.- The data presented in figure 9 ( $\delta_F = 0^\circ$ ; propellers removed) show that the combined effects of the nacelle-wing juncture, the wing-fuselage juncture, and the nacelle have a pronounced influence on the downwash that extends over the span of the horizontal tail. The downwash is greatest in the vicinity of the fuselage and smallest over the

area influenced by the nacelle-wing junctures. The flaps-deflected conditions,  $T_c = 0$ , also show the same general tendencies (figs. 12 and 14).

With power on there is an increase of downwash on the side of the downgoing propeller blade and a decrease on the side of the upgoing blade. The increase and decrease of downwash for the pusher-propelled airplane, as for a tractor-propelled airplane, appear to average out over the tail span. The values of  $\epsilon_{av}$  presented in table IV indicate that power has little effect on the variation of downwash with wing angle of attack.

Reference 1 shows that for a twin-engine, tractor-propelled airplane the effect of flap deflection was to reverse the effects of the upgoing and downgoing blades; that is, for flaps retracted the downgoing blades gave the greater downwash, whereas for flaps deflected the upgoing blades gave the greater downwash. Figures 11(d) and 15(c) indicate that this reversal did not occur for the pusher-propelled airplane.

Dynamic pressure.- The spanwise variation of  $q_t/q$  for the flaps-retracted propellers-removed condition is greatly influenced by the interference effects of the nacelle-wing juncture, the wing-fuselage juncture, and the nacelle (fig. 9). As the angle of attack is increased, the tail travels from the upper to the lower edge of the wake.

The values of  $q_t/q$  in the field influenced by the nacelle-wing juncture and the nacelle are greatly increased with power on, as shown by a comparison of figures 9 to 11. The increase of  $q_t/q$  becomes progressively greater with an increase of angle of attack because of a corresponding increase of  $T_c$  (fig. 11). The effect of the slipstream on the wake of the wing-fuselage juncture appears to be negligible. For all power conditions, there is a marked variation of  $q_t/q$  along the span of the horizontal tail. The data do not, however, indicate a severe distortion of the slipstream usually associated with a tractor-propelled airplane (reference 1).

The usual downward shift of the wake center line occurs with the flaps deflected, and, consequently, the tail enters the center of the wake at a higher angle of attack than it does with the flaps retracted. (Compare figs. 10 and 12.) Flap deflection causes a decided reduction in dynamic pressure and a widening of the wake.

Since the tail acts in a field of flow so predominantly influenced by the combined interference effects of the nacelle-wing juncture, the fuselage-wing juncture, and the nacelle, a condition of tail buffeting at moderate angles of attack may occur for any configuration. The low values of  $q_t/q$  associated with the interference effects indicate a separation of flow over the wing. These values agree with the results presented in figure 8. The lift curve presented in figure 8 for the flaps-retracted propellers-removed condition exhibits a break which can

be attributed to an interference burble either at the nacelle-wing or the fuselage-wing junctures or at both. Power tends to reduce the break.

### Average and Effective Values of Downwash and Dynamic Pressure

Downwash.- The results presented in table IV show that the values of  $\epsilon_{av}$  are approximately  $1^\circ$  to  $2^\circ$  greater than the values of  $\epsilon_{eff}$ . In order to determine the reasons for the differences between effective and average values of  $\epsilon$ , a study of the assumptions made in both methods of calculations must be made.

When computations of  $\epsilon_{eff}$  are made from force and moment data, the basic assumption is that the difference between tail-on and tail-off pitching moments is a measure of the tail lift attributable to the complete tail area (fig. 17(a)). Theoretically, however, the loading is more closely represented by figure 17(b).

Although pressure-distribution tests were not obtained for the present model, the data of reference 2 for a canard-type airplane (negligible effects of  $q_t/q$ ) have indicated the loading of the fuselage induced by the tail to be considerably less than the theoretical loading (fig. 17(b)). In the present case it is therefore not unlikely to suppose that, because of the extremely thick fuselage boundary layer over the rear of the fuselage, the loading shown in figure 17(c) would be a closer approximation to the actual loading than that shown in figure 17(b). The effect of a change in stabilizer setting would be felt outboard of the fuselage (fig. 17(d)). On the basis of the assumed loading (figs. 17(c) and 17(d)), the effective downwash angles computed from force and moment data would consequently be approximately the effective downwash angle  $\epsilon_{eff}$  acting over the span of the tail outboard of the fuselage.

There are two basic assumptions made when air-stream-survey values of  $\epsilon_{av}$  are obtained by equation (1). First, the downwash measured on each side of the fuselage is assumed to extend across the fuselage; and, second, the distribution of lift on the tail is assumed to be proportional to the local chords of the tail. When weighted according to the tail chord over the area intercepted by the fuselage, the rather large values of  $\epsilon$  in the vicinity of the fuselage therefore have a predominant influence on the value of  $\epsilon_{av}$ . A comparison between values of  $\epsilon_{av}$  obtained when weighted according to the chord distribution and when weighted according to an isolated-tail carry-over lift distribution showed negligible differences. The assumed loading for the lift of the tail outboard of the fuselage plus the lift of the fuselage induced by the tail (fig. 17(c)) indicates that, although the chord distribution satisfactorily represents the lift distribution outboard of the fuselage, it does not represent the lift distribution over the fuselage. As a result, the air-stream-survey data were integrated only over the tail

span outboard of the fuselage (fig. 17(b)). Approximately one-half of the original discrepancy (table IV) between  $\epsilon_{av}$  and  $\epsilon_{eff}$  remained and indicated that the loading over the center part of the tail was even less than that shown in figure 17(c).

An empirical formula is introduced by which an effective span for integrating air-stream-survey data can be obtained. This formula has been based on the assumption that a change in  $C_{L\alpha_t}$  between isolated-

tail tests and complete-model tests may be assumed to be an effective change in aspect ratio. Thus

$$(b_t)_{eff} = b_t \sqrt{\frac{1}{A_t \left[ \frac{(C_{L\alpha_t})_{iso}}{(C_{L\alpha_t})_{eff}} \left( \frac{\pi}{57.3a_o} + \frac{1}{A_t} \right) - \frac{\pi}{57.3a_o} \right]}} \quad (2)$$

The air-stream-survey data of the present paper were integrated over each semispan from  $\frac{b_t - (b_t)_{eff}}{2}$  to  $\frac{b_t}{2}$  and the resulting values of  $\epsilon_{av}'$  are presented in table IV. Very close agreement was obtained between  $\epsilon_{av}'$  and  $\epsilon_{eff}$ .

The reliability of using equation (2) has not been established by sufficient test application. Inasmuch as a knowledge of the values of  $(C_{L\alpha_t})_{eff}$  and  $(C_{L\alpha_t})_{iso}$  is required, the method for determining values of  $\epsilon_{av}'$  from air-stream-survey data is limited to tests for which complete model and isolated tail data are also available. Use of equation (2) has indicated, however, that force and moment data neglect the rather large effects attributed to the fuselage when values of  $\epsilon_{eff}$  are computed. The effect of the fuselage should therefore be accounted for when air-stream surveys are used to obtain  $\epsilon_{av}$ .

Air-stream-survey data and force and moment data were obtained in the Langley 19-foot pressure tunnel for a four-engine, photoreconnaissance, tractor-propelled airplane which had the horizontal tail located above the fuselage on the vertical tail. The values of  $\epsilon_{av}$  were within experimental accuracy of values of  $\epsilon_{eff}$ . The computed value of  $(b_t)_{eff}$  was approximately equal to  $b_t$  and, hence, showed that equation (2) was satisfactory for an extreme condition.

Dynamic pressure.- A discussion similar to that presented herein on downwash can be used to show that force and moment data also determine an effective dynamic-pressure ratio  $(q_t/q)_{\text{eff}}$  over the tail span effectively outboard of the fuselage.

The discrepancies between  $(q_t/q)_{\text{av}}$  and  $(q_t/q)_{\text{eff}}$  were only slightly reduced, however, when values of  $(q_t/q)_{\text{av}}$  were obtained (table IV). It is quite possible that the remaining disagreement is due, in a large part, to the accuracy with which  $(q_t/q)_{\text{eff}}$  can be obtained from force and moment data. Since rather small values of  $\Delta l_t$  are used to obtain  $C_{m_{l_t}}$ , the balance system must provide very accurate measurements of  $C_m$ . For the present tests, the low dynamic pressure and the sensitivity of the balance system combine to give an estimated accuracy of  $(q_t/q)_{\text{eff}}$  of approximately 6 percent. The main result indicated by these data is that force and moment data do not provide a means for accurately determining  $(q_t/q)_{\text{eff}}$  if the forces and moments are obtained at low speeds and are measured by a typical tunnel balance system.

#### CONCLUDING REMARKS

The results of air-stream surveys and comparison of average and effective values of downwash and dynamic pressure at the tail of a high-wing, six-engine, powered, pusher-propelled model indicated:

1. The average values of downwash obtained from air-stream surveys were approximately  $1^\circ$  to  $2^\circ$  greater than the effective values obtained from force and moment data. A concept that the part of the tail intercepted by the fuselage contributed little, if any, to the evaluation of the effective values of downwash angle from force and moment data was used to obtain an empirical formula by which average values of downwash angle obtained from air-stream surveys could be made to agree satisfactorily with effective values.
2. The average values of dynamic-pressure ratio obtained by the use of the empirical method did not agree satisfactorily with the effective values of dynamic-pressure ratio obtained from force and moment data. This disagreement was attributed to the accuracy with which effective values of dynamic-pressure ratio could be obtained from force and moment data.
3. For all flap conditions (retracted and deflected) the tail passed into the center of the wake at moderate to high angles of attack.
4. The nacelle-wing juncture (no fillet), the fuselage-wing juncture (no fillet), and the nacelle had a pronounced effect on the flow at the tail.

5. The severe distortion of the slipstream usually associated with a tractor-propelled airplane did not occur.

6. When the flaps were deflected, the effects of the upgoing and downgoing blades were not reversed as previously reported for a tractor airplane.

Langley Memorial Aeronautical Laboratory  
National Advisory Committee for Aeronautics  
Langley Field, Va.

#### REFERENCES

1. Sweberg, Harold H.: The Effect of Propeller Operation on the Air Flow in the Region of the Tail Plane for a Twin-Engine Tractor Monoplane. NACA ARR, Aug. 1942.
2. Sandahl, Carl A., and Vollo, Samuel D.: Wind-Tunnel Investigation of the Air Load Distribution on Two Combinations of Lifting Surface and Fuselage. NACA TN No. 1295, 1947.

TABLE I  
DESIGN CHARACTERISTICS OF A SIX-ENGINE,  
PUSHER-PROPELLED, POWERED MODEL

Wing	
Root chord	
Section . . . . .	NACA 63(420)-422
Chord, in. . . . .	28.52
Angle of incidence, deg . . . . .	3
Tip chord (theoretical)	
Section . . . . .	NACA 63(420)-517
Chord, in. . . . .	7.14
Angle of incidence, deg . . . . .	1
Area, sq ft . . . . .	24.35
Span, in. . . . .	197.14
Aspect ratio . . . . .	11.09
Mean aerodynamic chord (M.A.C.), in. . . . .	20.05
Spanwise location of M.A.C., in. . . . .	39.07
Sweepback	
Leading edge, deg . . . . .	15.101
Trailing edge, deg . . . . .	3
Taper ratio . . . . .	4
Dihedral (from wing root-chord plane), deg . . . . .	2
Washout (aerodynamic), deg . . . . .	2
Flaps	
Chord, in. . . . .	5.36
Deflections, deg . . . . .	0, 20, and 40
Area, sq in.	
Between outboard and center nacelles . . . . .	58.75
Between center and inboard nacelles . . . . .	57.63
Between inboard nacelle and fuselage . . . . .	72.72
Span, in.	
Between outboard and center nacelles . . . . .	10.97
Between center and inboard nacelles . . . . .	10.76
Between inboard nacelle and fuselage . . . . .	13.56
Fuselage	
Length, ft . . . . .	11.64
Maximum diameter, in. . . . .	10.71
Maximum frontal area, sq in. . . . .	90.14



TABLE I - Concluded  
 DESIGN CHARACTERISTICS OF A SIX-ENGINE,  
 PUSHER-PROPELLED, POWERED MODEL - Concluded

Horizontal tail	
Root chord	
Section . . . . .	NACA 0015
Chord, in. . . . .	17.31
Tip chord (theoretical)	
Section . . . . .	NACA 0015
Chord, in. . . . .	5.79
Total area (projected), sq ft . . . . .	4.99
Span, in. . . . .	62.91
Aspect ratio . . . . .	5.5
Mean aerodynamic chord, in. . . . .	12.58
Taper ratio . . . . .	3
Tail length ( $\frac{1}{4}$ chord of wing M.A.C. to $\frac{1}{4}$ chord of tail M.A.C.), in. . . . .	62.00
Dihedral, deg . . . . .	0
Sweepback (elevator hinge line), deg . . . . .	0
Elevator area (total), sq ft . . . . .	2.32
Vertical distance of elevator hinge line below wing-root-chord plane, in. . . . .	0.033
Vertical tail	
Root chord	
Section . . . . .	NACA 0015
Chord, in. . . . .	23.21
Tip chord	
Section . . . . .	NACA 0012
Chord, in. . . . .	8.43
Total area (including dorsal), sq ft . . . . .	2.77
Span, in. . . . .	22.86
Aspect ratio . . . . .	1.475
Taper ratio . . . . .	2.75
Tail length ( $\frac{1}{4}$ chord of wing M.A.C. to rudder hinge line), in. . . . .	68.11
Rudder (area), sq ft . . . . .	1.15
Propellers	
Number . . . . .	6
Number of blades per propeller . . . . .	3
Diameter, ft . . . . .	1.36
Type . . . . .	Curtiss 1129-IC6-24 (left hand)



TABLE II  
SIMULATED FULL-SCALE POWER CONDITIONS

Power	Brake horsepower (per engine)	Airplane gross weight (lb)	Altitude (ft)	Engine speed (rpm)	Gear ratio	Propeller speed (rpm)
100-percent rated power	2500	265,000	Sea level	2550	0.29	725
75-percent rated power	1875	265,000	10,000	2100	.29	609
50-percent rated power	1250	265,000	Sea level	2100	.29	609
Zero thrust, $T_c = 0$	Low	175,000 to 350,000	Sea level to maximum altitude	Low	.29 and .50	Low



TABLE III  
 CONTOUR CHARTS OF DOWNWASH AND  
 DYNAMIC-PRESSURE RATIOS

Figure	$\delta_f$ (deg)	Power	Slots	Landing gear	$\alpha_w$ (deg)
9	0	Propellers removed	Closed	Off	0.2, 3.4, 7.7, 11.8, 16.0
10	0	$T_c = 0$	--do--	Off	0.2, 3.4, 7.7, 11.9, 16.1
11	0	Rated power	--do--	Off	0.2, 3.4, 7.8, 12.0, 16.2
12	20	$T_c = 0$	Open	On	0.5, 4.7, 9.0, 13.2
13	20	0.75 rated power	--do--	On	0.5, 4.8, 9.1, 13.4
14	40	$T_c = 0$	--do--	On	0.7, 5.0, 9.2, 13.5
15	40	0.50 rated power	--do--	On	0.7, 5.0, 9.3, 13.6



TABLE IV  
VALUES OF DYNAMIC-PRESSURE RATIO AND DOWNWASH ANGLE

Power condition	$\alpha$ (deg)	$(q_t/q)_{av}$	$\epsilon_{av}$	$(q_t/q)_{off}$	$\epsilon_{off}$	$(q_t/q)_{av}'$	$\epsilon_{av}'$
$\delta_F = 0^\circ$							
Propellers removed	0.2	0.97	3.0	1.00	1.2	1.00	1.5
	3.4	.95	4.1	1.00	2.2	.98	2.6
	7.7	.90	5.5	.96	3.8	.94	3.9
	11.8	.80	7.2	.88	5.2	.85	5.2
	16.0	.88	9.6	.93	6.8	.91	6.8
$T_c = 0$	.2	.96	2.9	1.01	1.3	.98	1.5
	3.4	.98	4.0	1.05	2.4	1.00	2.6
	7.7	.93	5.5	.96	3.8	.96	4.0
	11.9	.83	6.9	.84	5.3	.87	5.1
	16.1	.90	9.5	.92	7.1	.94	7.1
Rated power	.2	.95	3.0	1.05	1.3	.97	1.6
	3.4	1.02	4.0	1.07	2.4	1.04	2.5
	7.8	1.04	5.4	1.05	3.7	1.10	3.8
	12.0	1.08	7.0	1.07	5.7	1.15	5.7
	16.2	----	---	----	---	----	---
$\delta_F = 20^\circ$							
$T_c = 0$	0.5	0.98	6.2	0.88	4.3	0.98	4.3
	4.7	.93	7.9	.92	5.5	.95	5.6
	9.0	.85	9.5	.94	7.2	.89	7.1
	13.2	.83	11.0	.91	8.6	.89	8.3
0.75 rated power	.5	.99	6.2	.93	4.4	.99	4.2
	4.8	.98	7.8	1.03	5.7	1.02	5.7
	9.1	1.00	8.5	1.20	7.2	1.11	6.6
	13.4	1.05	9.6	1.37	8.6	1.20	7.6
$\delta_F = 40^\circ$							
$T_c = 0$	0.7	1.02	7.5	0.97	4.4	1.02	4.4
	5.0	.97	9.4	1.01	7.0	.99	7.1
	9.2	.88	11.6	1.02	8.6	.94	8.8
	13.5	.81	11.7	.97	10.1	.86	10.1
0.50 rated power	.7	.99	7.9	.95	5.9	1.01	5.7
	5.0	1.00	9.8	1.04	7.3	1.04	7.3
	9.3	.99	11.0	1.17	8.7	1.08	8.6
	13.6	1.00	11.6	1.20	10.3	1.08	10.3

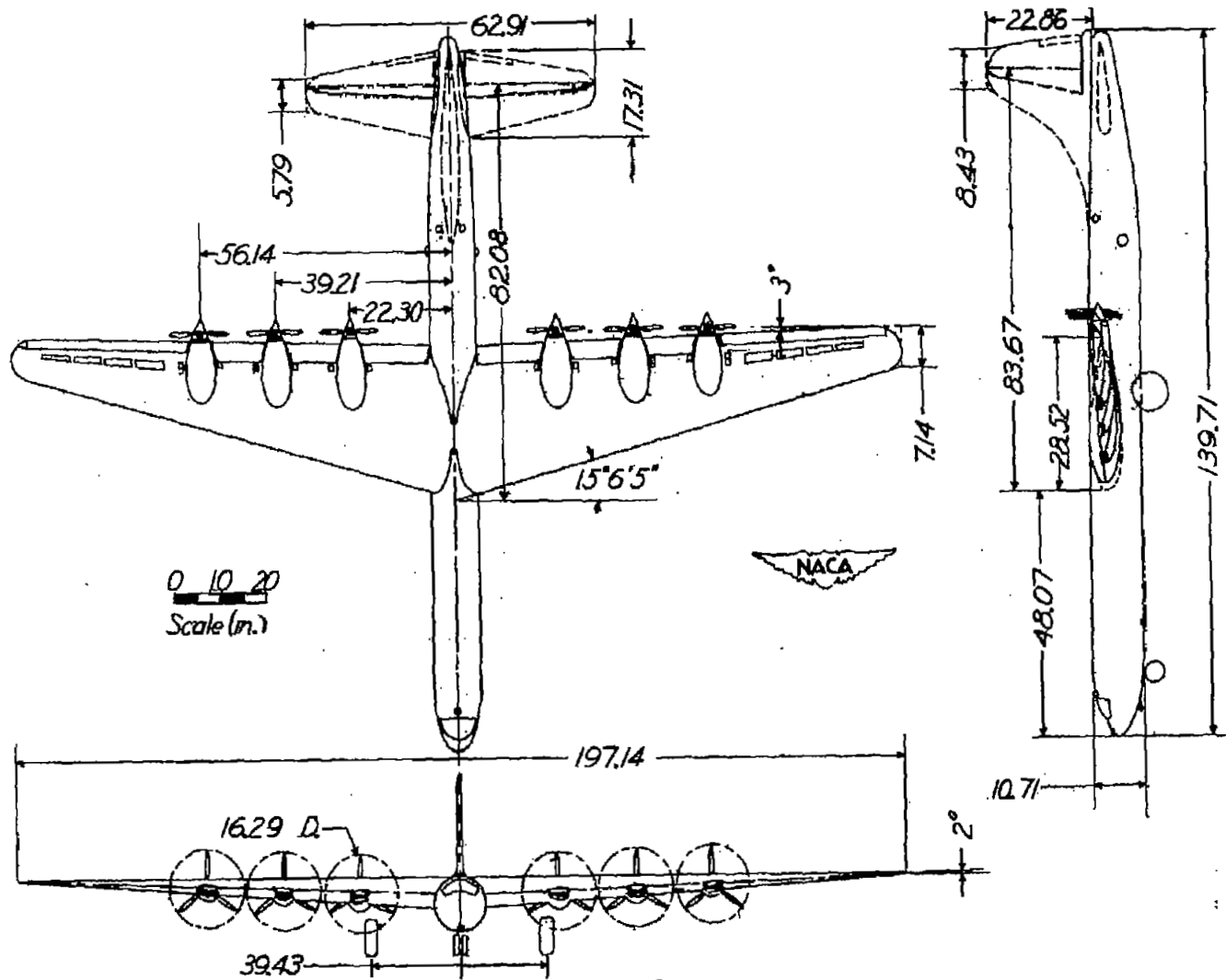
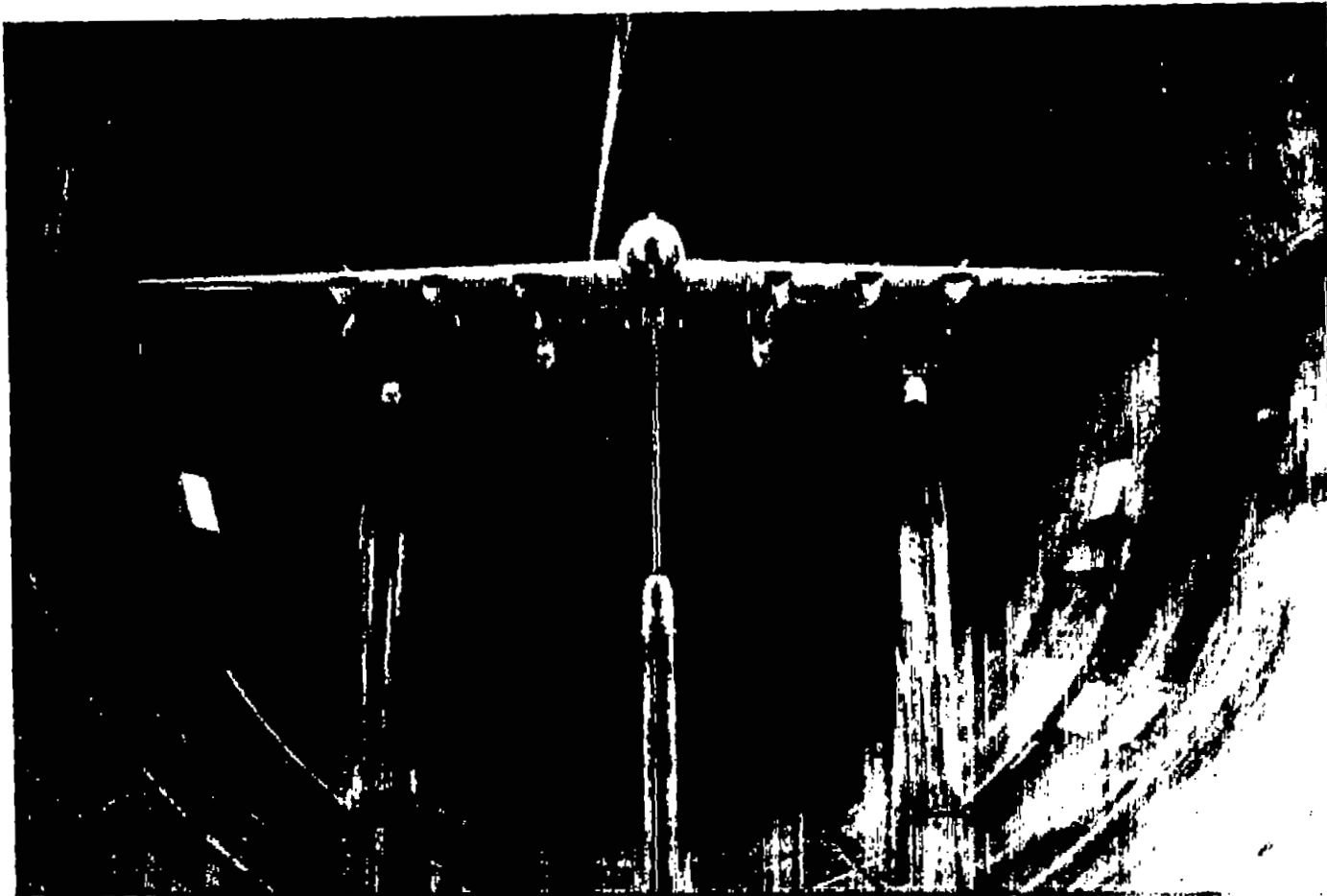


Figure 1.- Three-view drawing of the  $\frac{1}{14}$ -scale model; left-hand propeller rotation. (All dimensions are in inches.)



(a) Front view.

Figure 2.- The  $\frac{1}{14}$ -scale powered model mounted in Langley 19-foot pressure tunnel.



L-40575

2

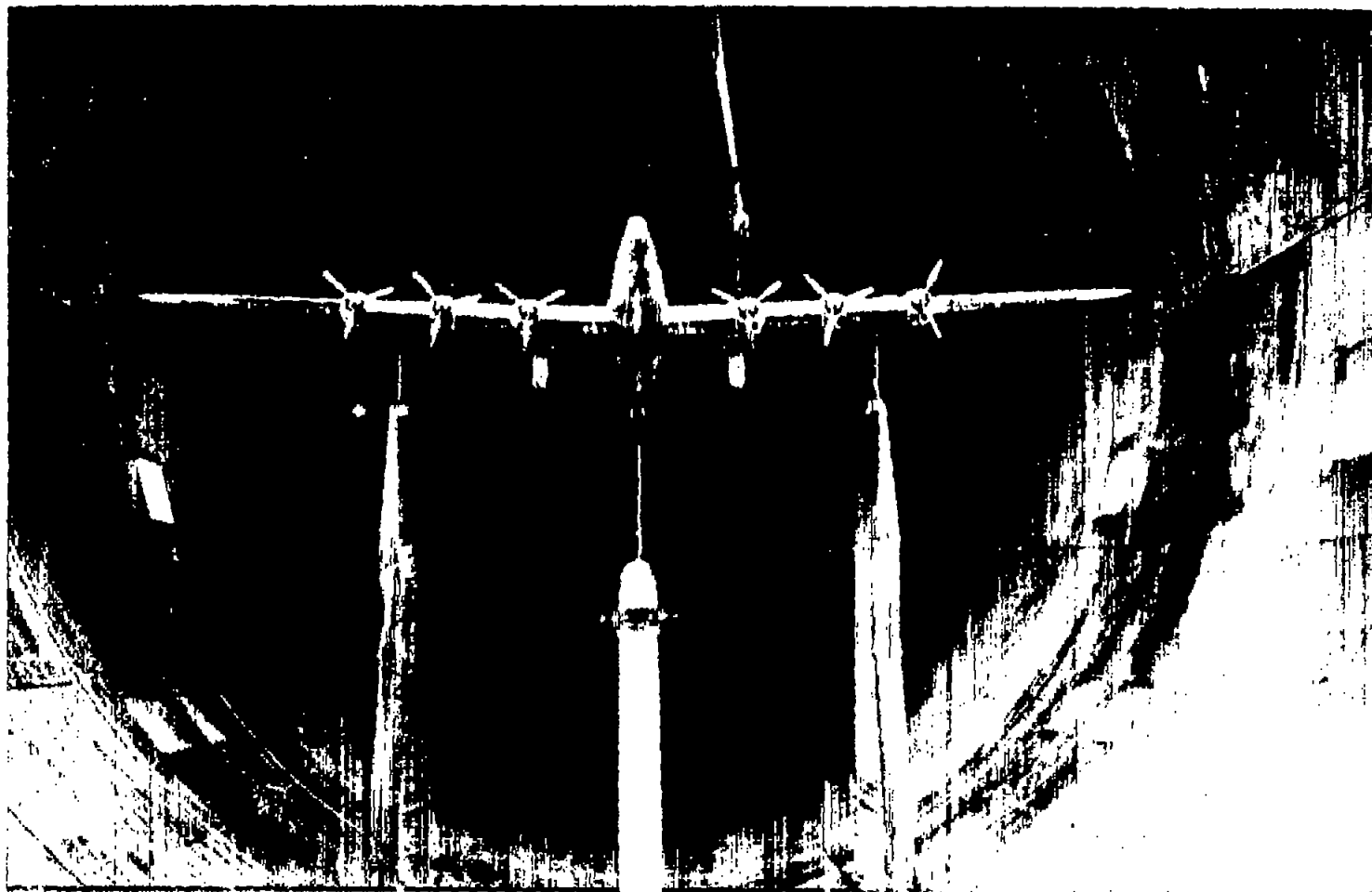
3

4

5

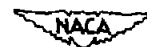
6

7



(b) Rear view.

Figure 2.- Concluded.



L-40576



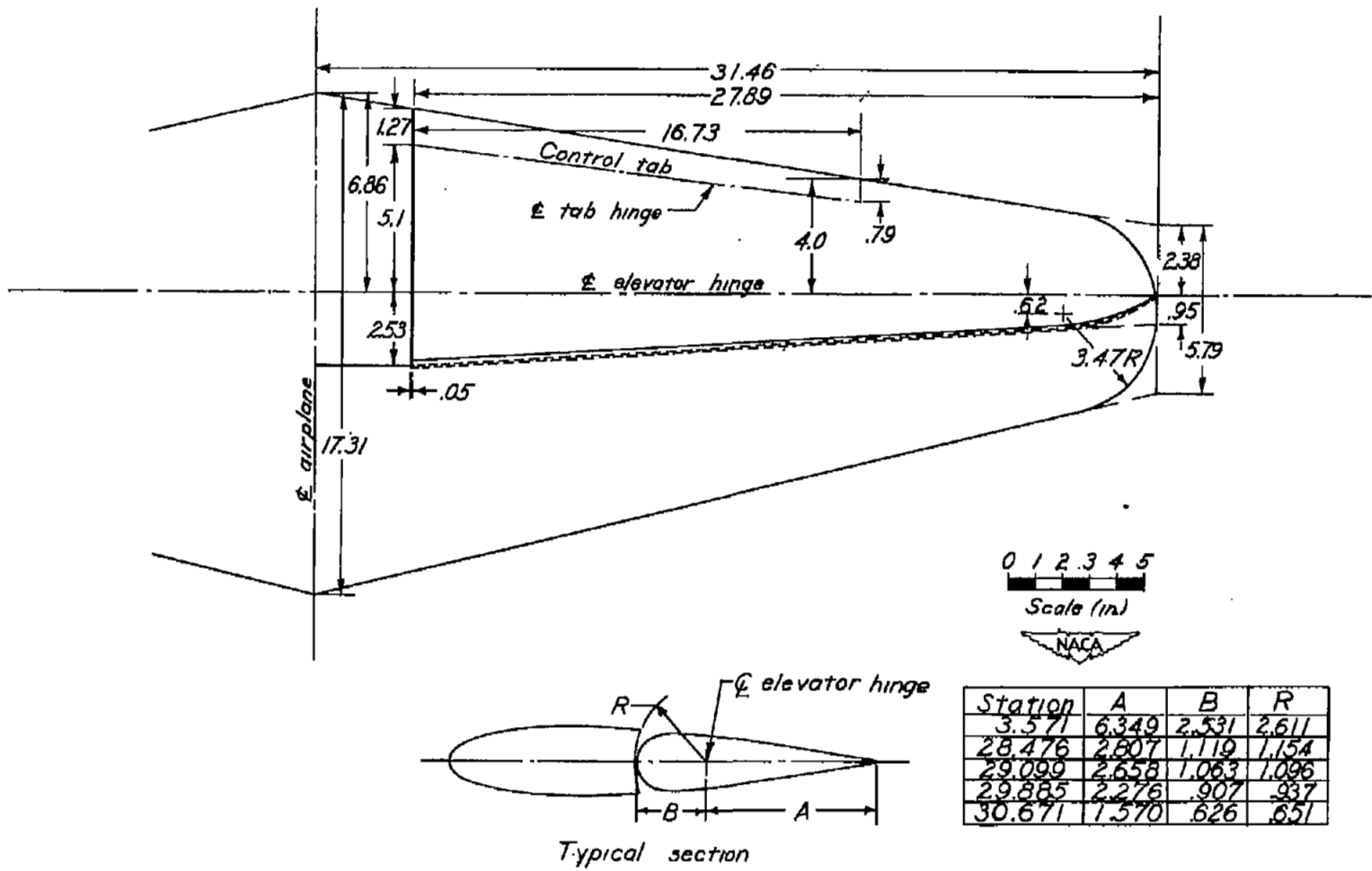
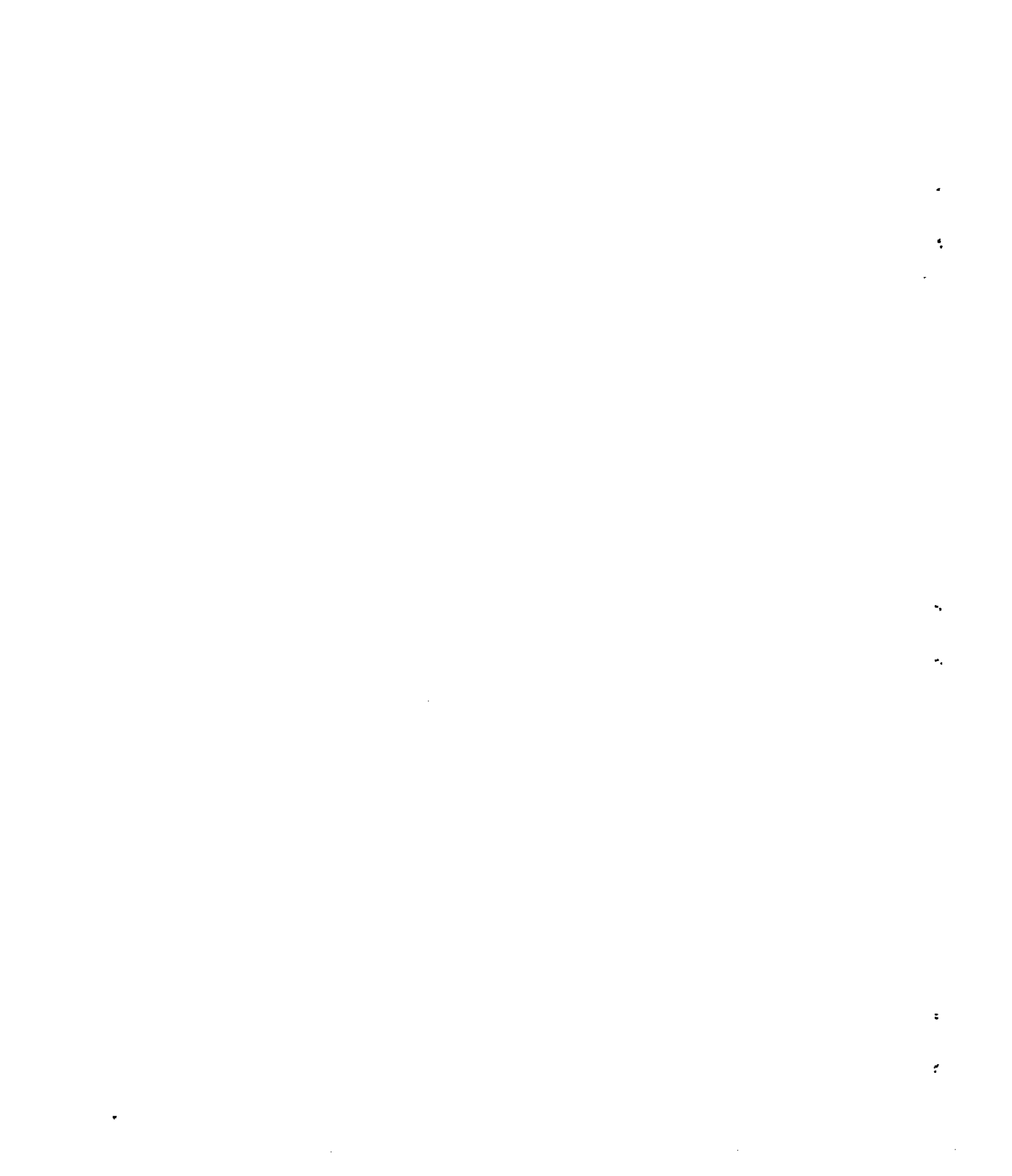
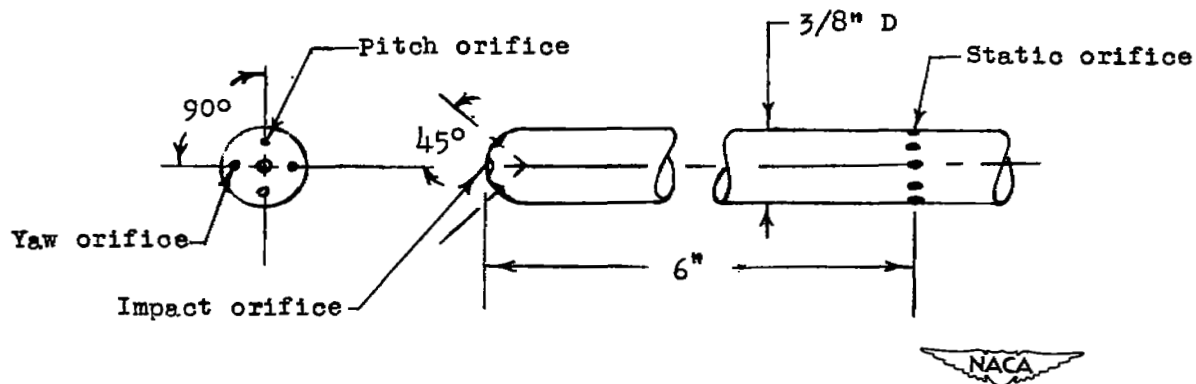


Figure 3.- Details of horizontal tail. (All dimensions are in inches.)





(a) Close up of rake head.



(b) Sketch of tube head.

Figure 4.- Air-stream survey rake for Langley 19-foot pressure tunnel.

1

2

3

4

5

6

7

8

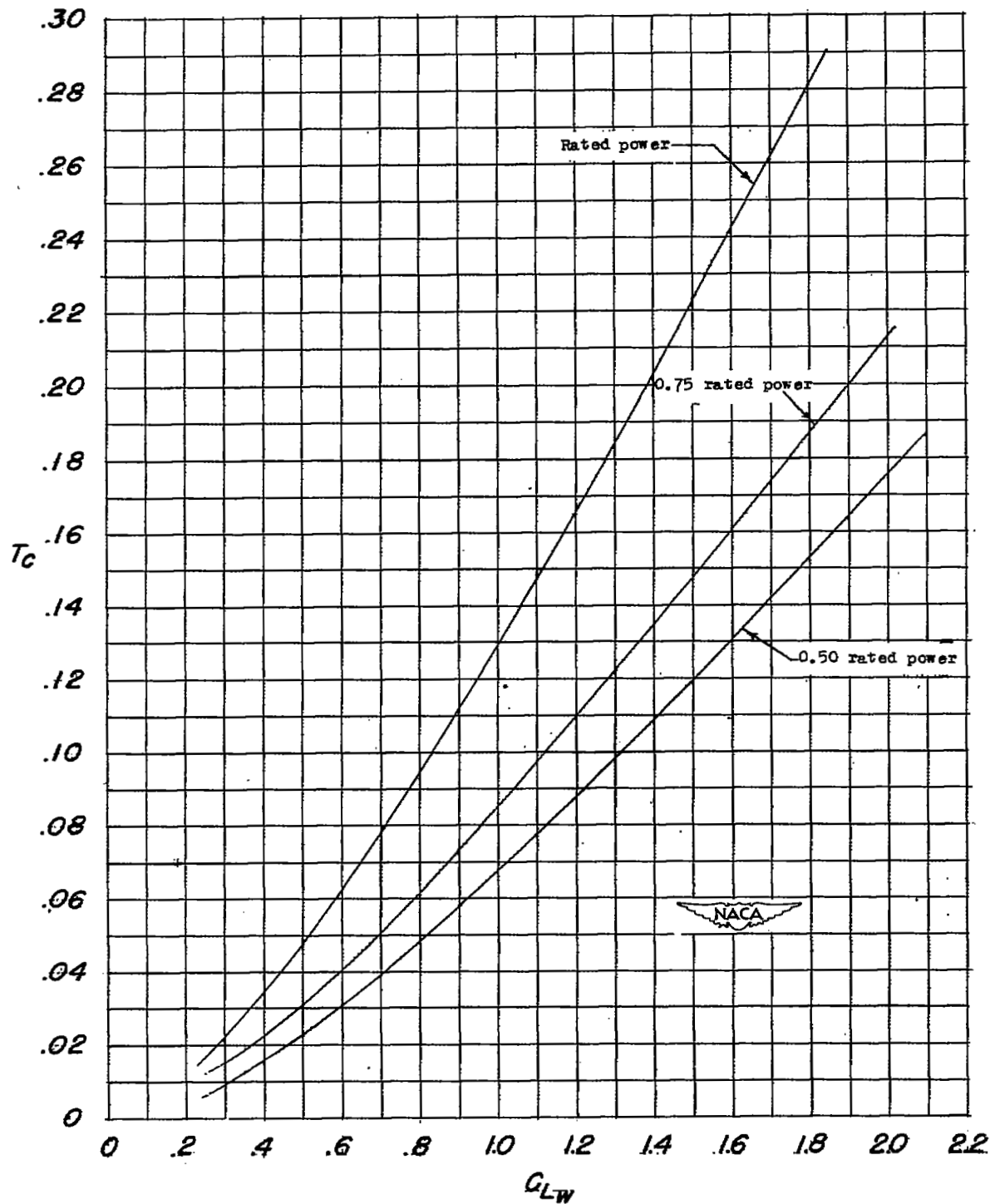


Figure 5.- Variation of thrust disk-loading coefficient with wing lift coefficient for several power conditions. Single-propeller operation.

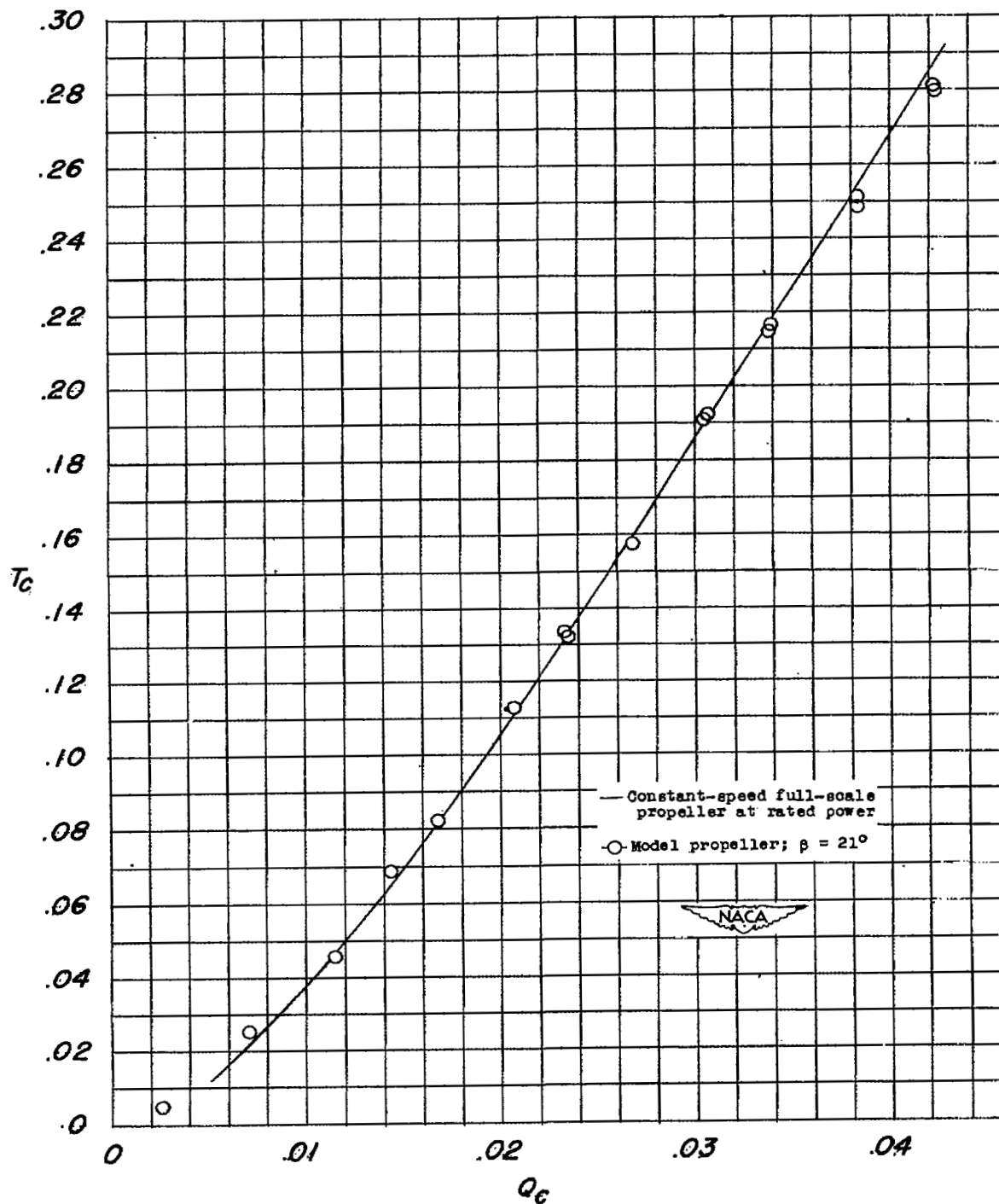


Figure 6.- Variation of thrust disk-loading coefficient with torque disk-loading coefficient for the full-scale constant-speed propeller and the  $\frac{1}{14}$ -scale-model constant-pitch propeller. Single-propeller operation.

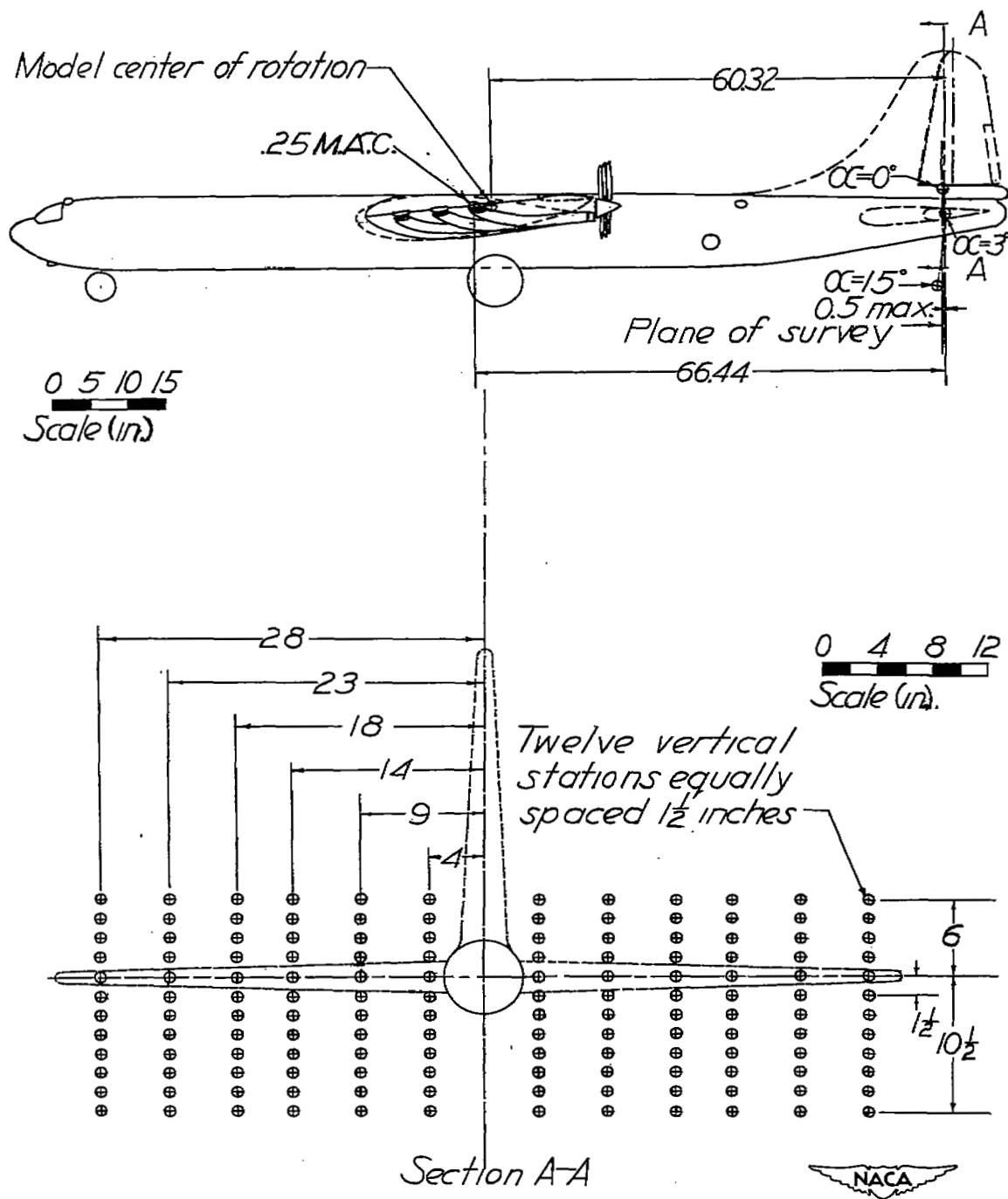


Figure 7.- Air-stream-survey plane for tests of the  $\frac{1}{14}$ -scale model.  
(All dimensions are in inches.)

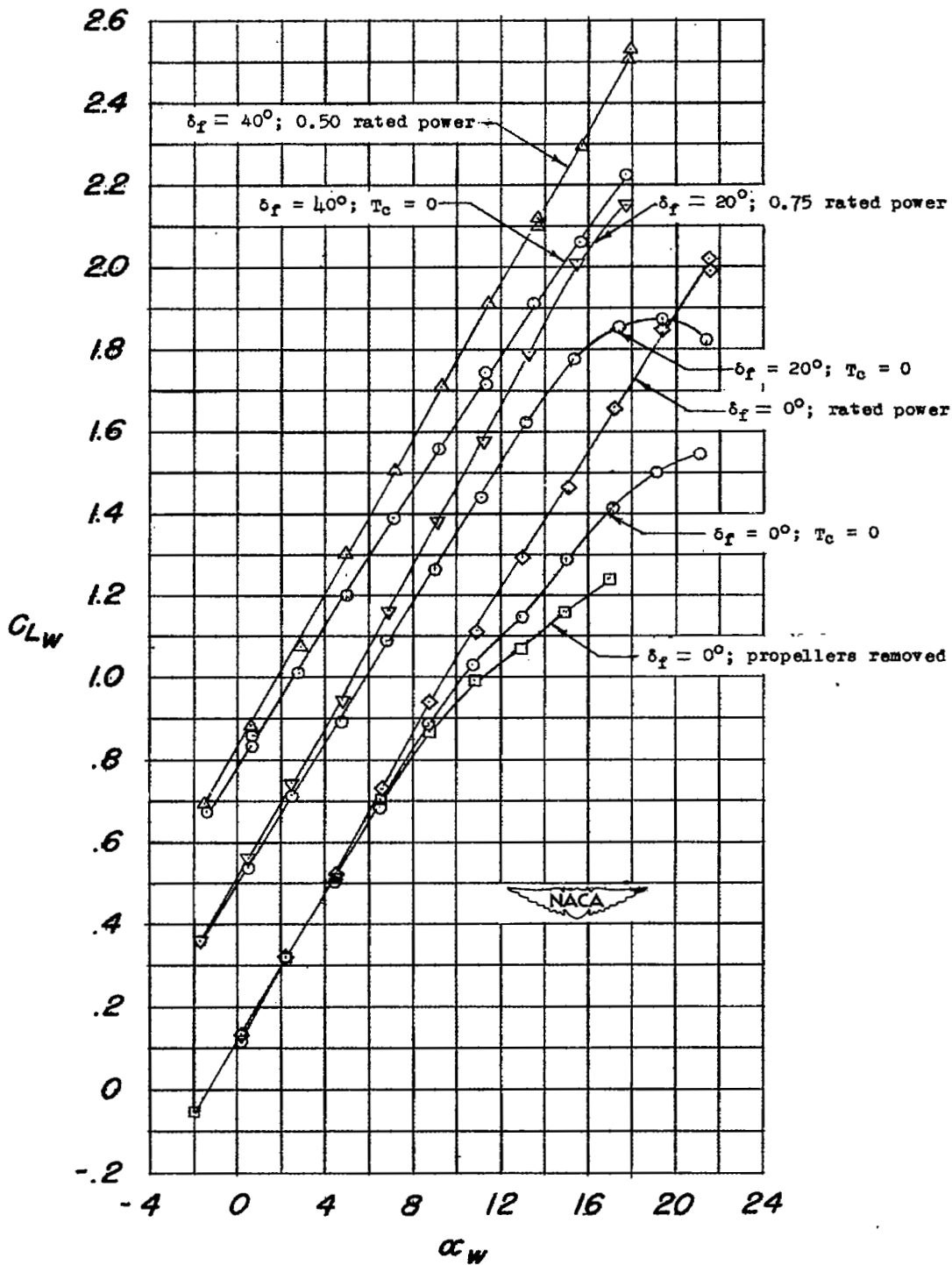
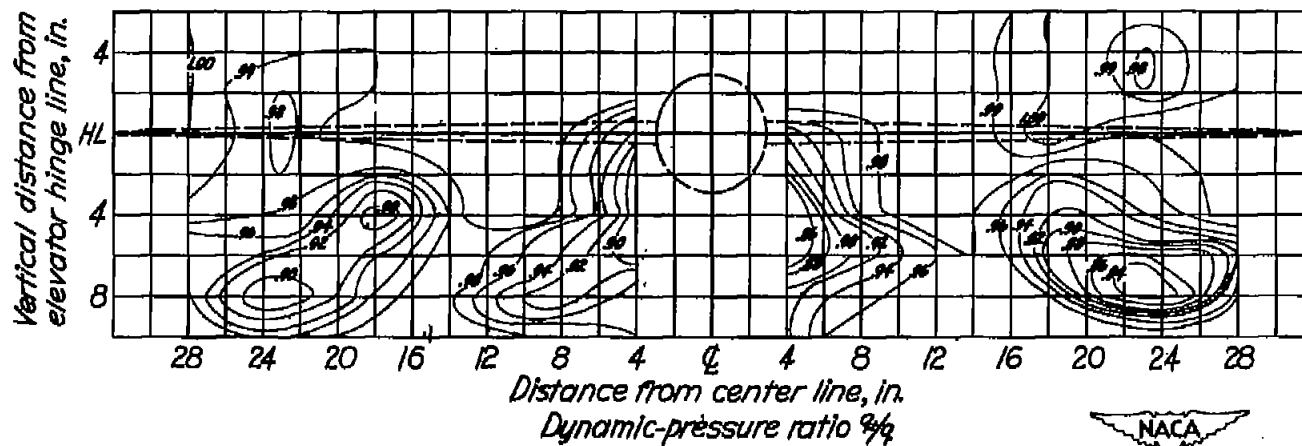
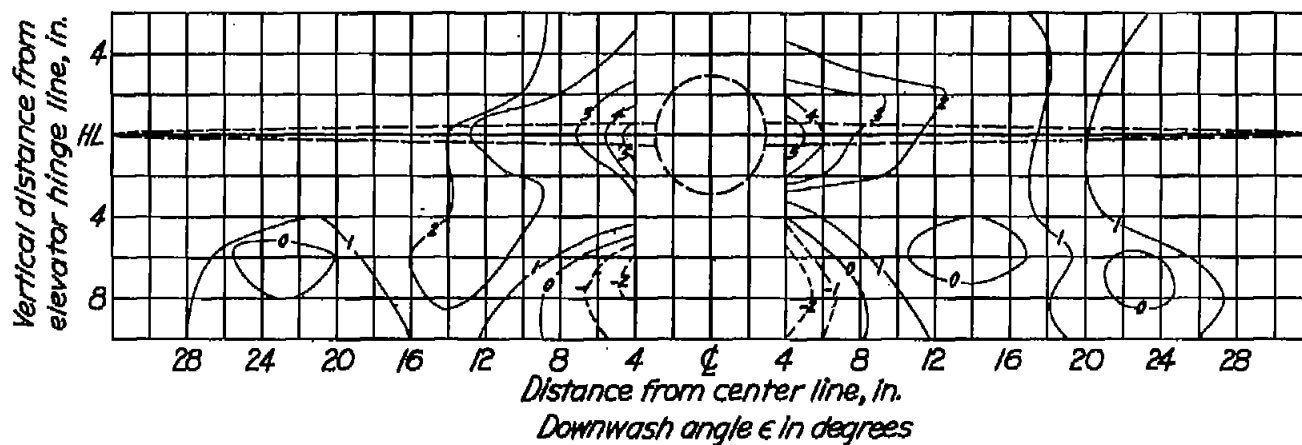
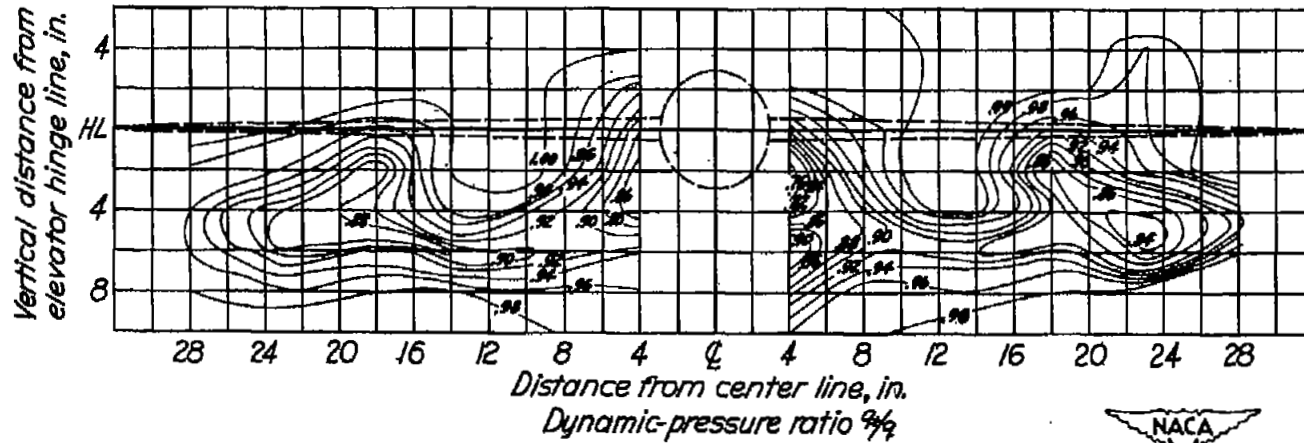
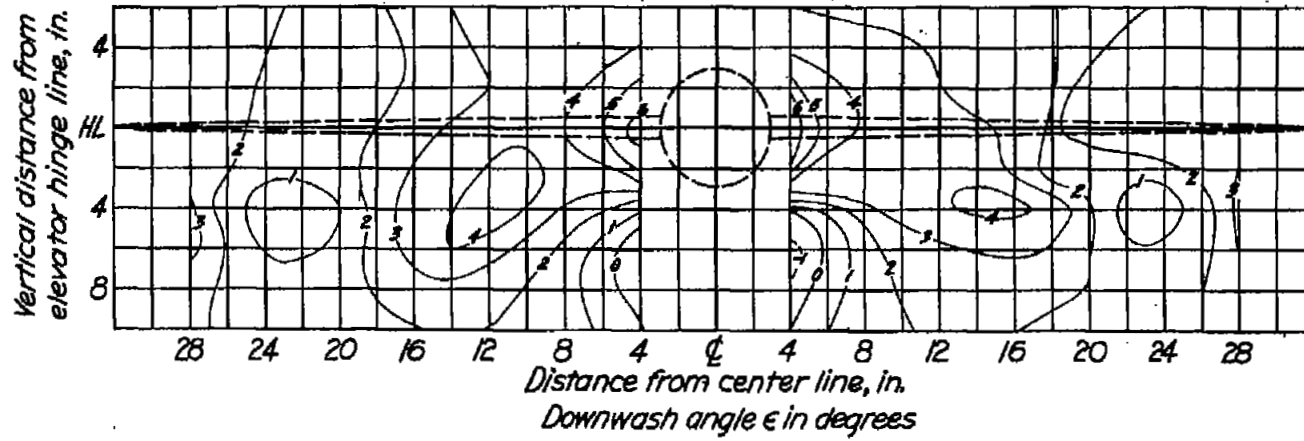


Figure 8.- Tail-off lift curves for various flap deflections and power conditions.



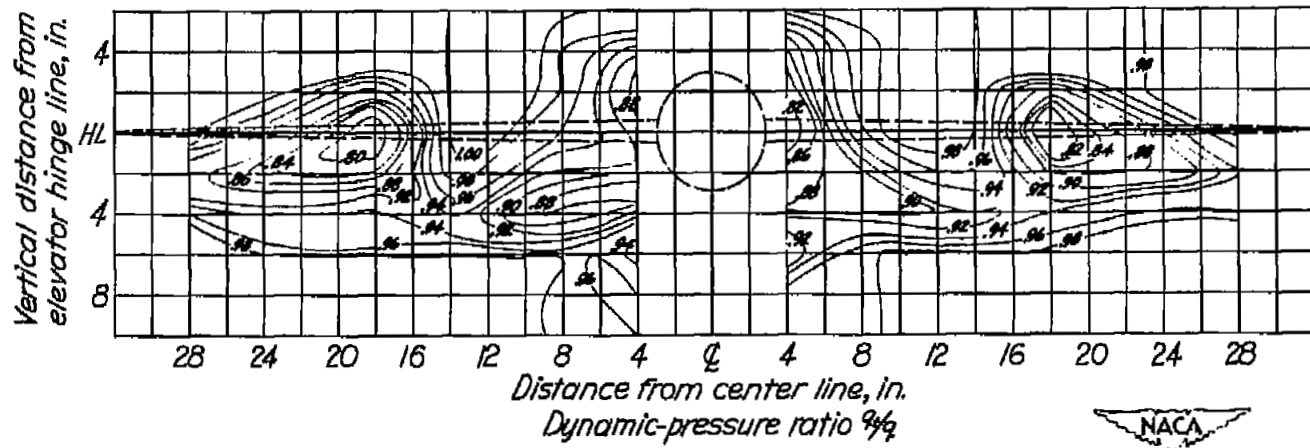
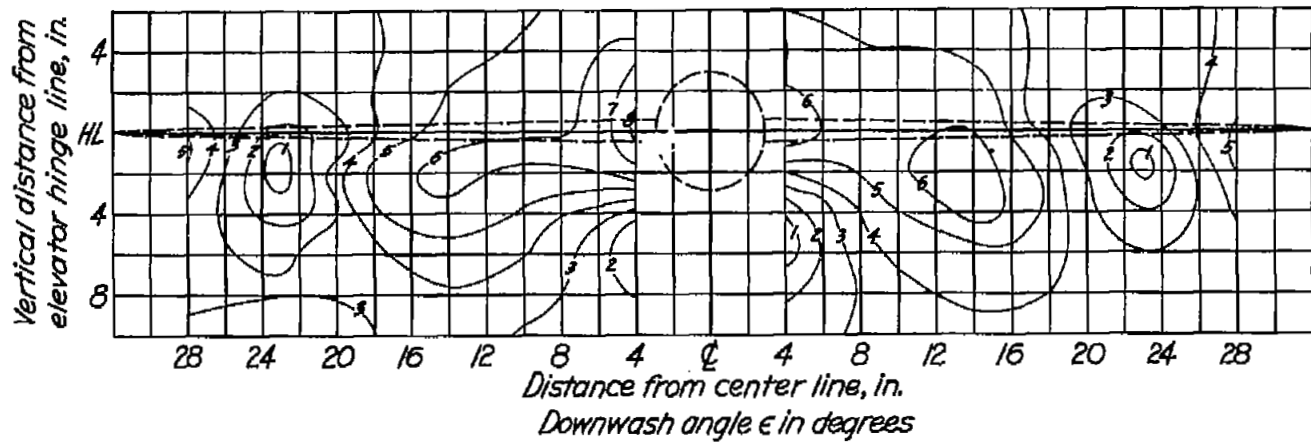
(a)  $\alpha_w = 0.2^\circ$ .

Figure 9.- Downwash angles and dynamic-pressure ratios in the vertical plane of the elevator hinge line. View looking upstream.  $\delta_f = 0^\circ$ ; propellers removed;  $R \approx 2,440,000$ .



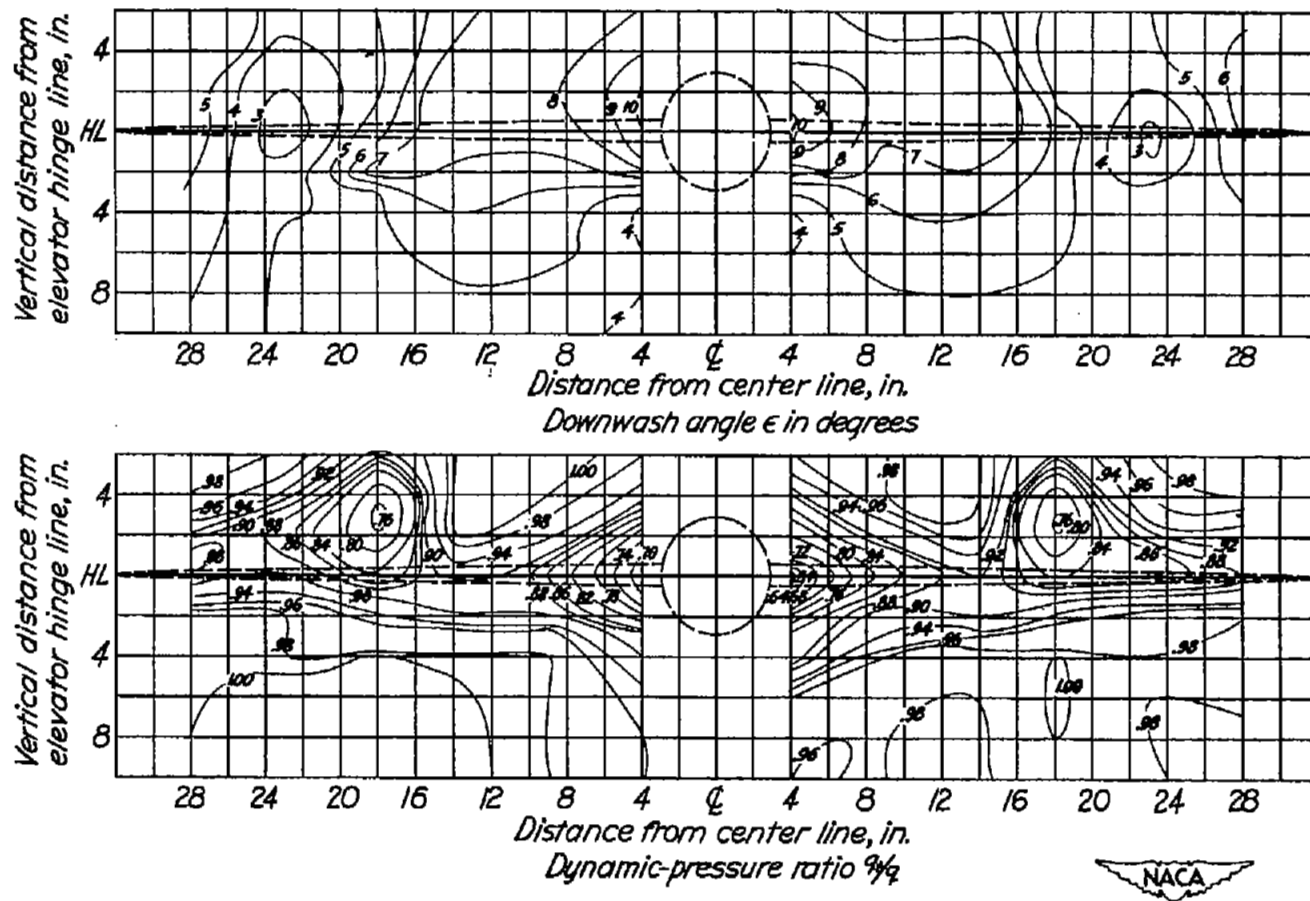
(b)  $\alpha_w = 3.4^\circ$ .

Figure 9.- Continued.



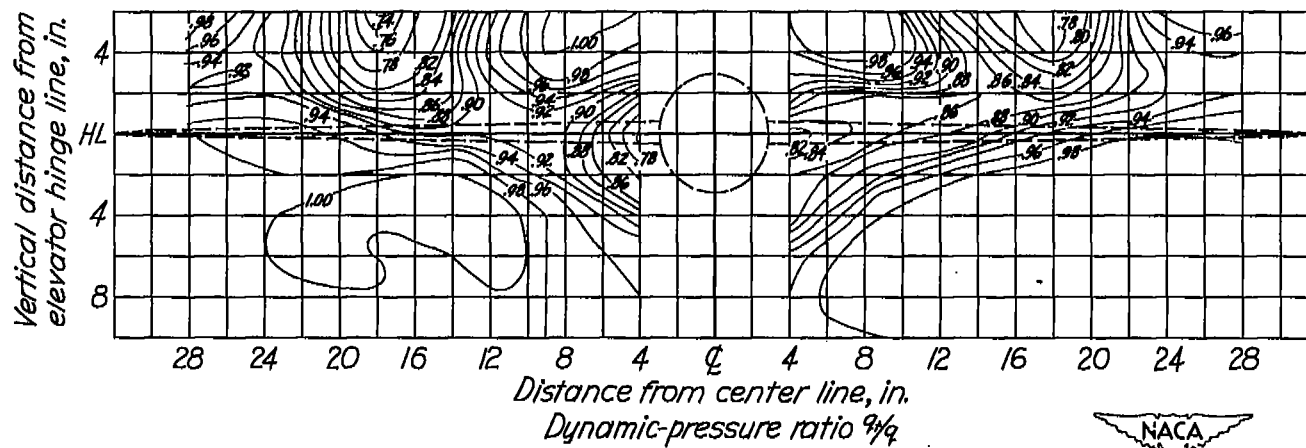
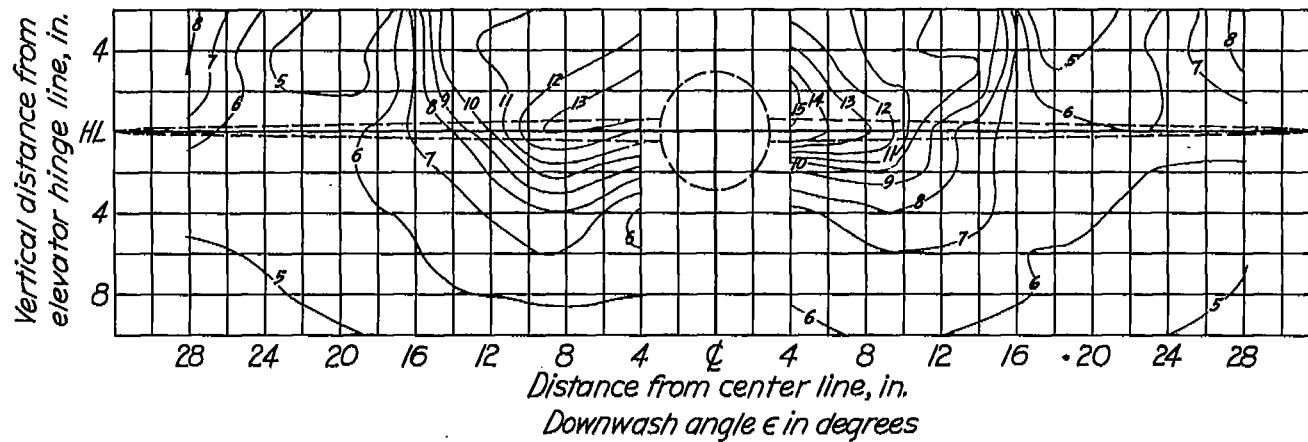
(c)  $\alpha_w = 7.7^\circ$ .

Figure 9.- Continued.



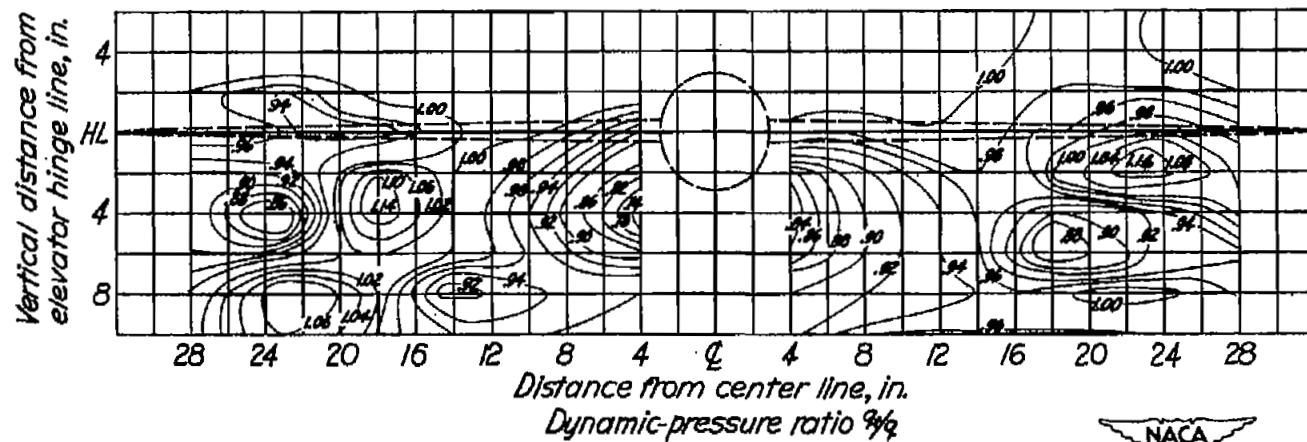
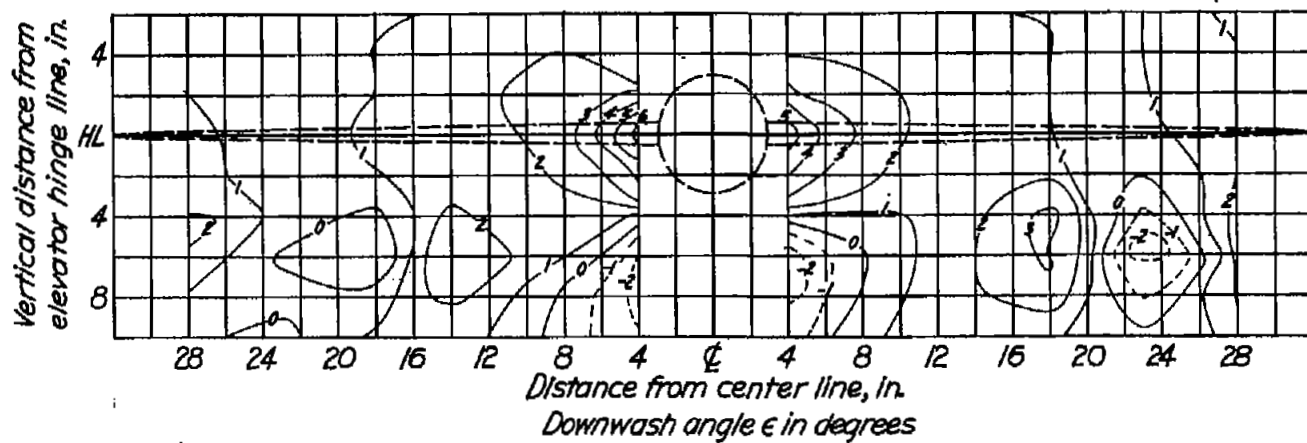
$$(d) \alpha_w = 11.8^\circ.$$

Figure 9.- Continued.



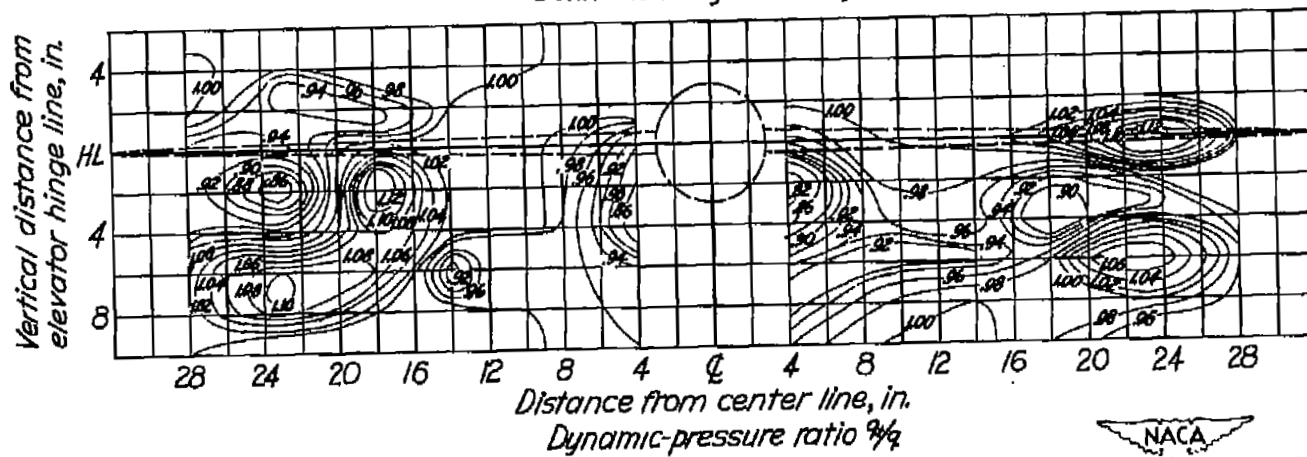
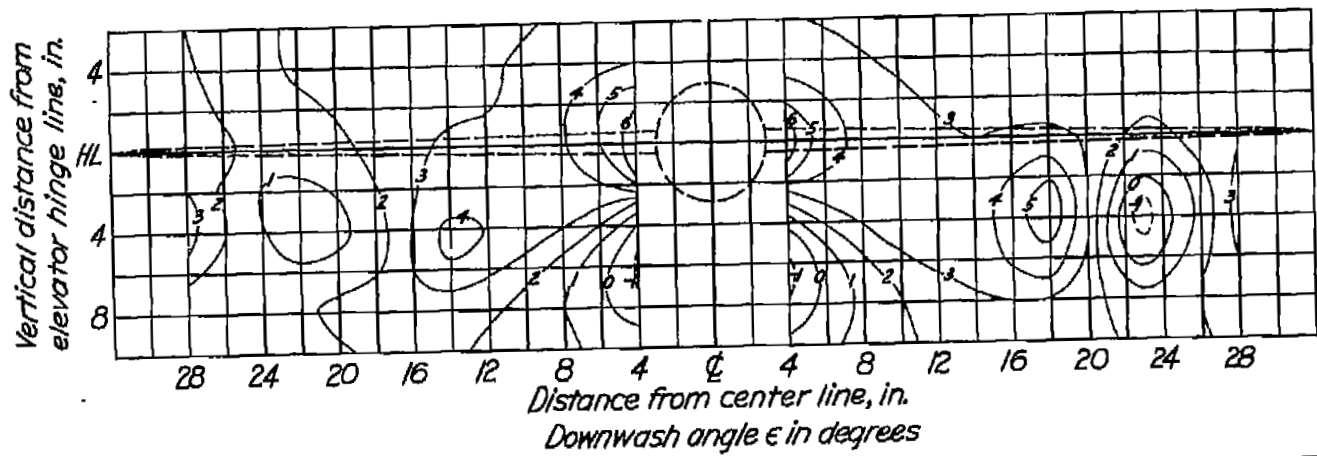
(e)  $\alpha_w = 16.0^\circ$ .

Figure 9.- Concluded.



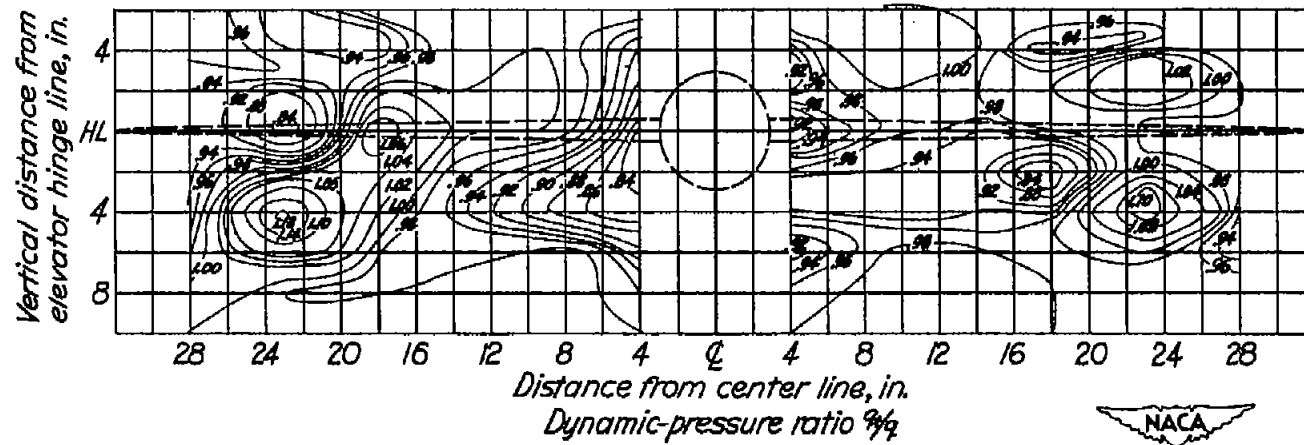
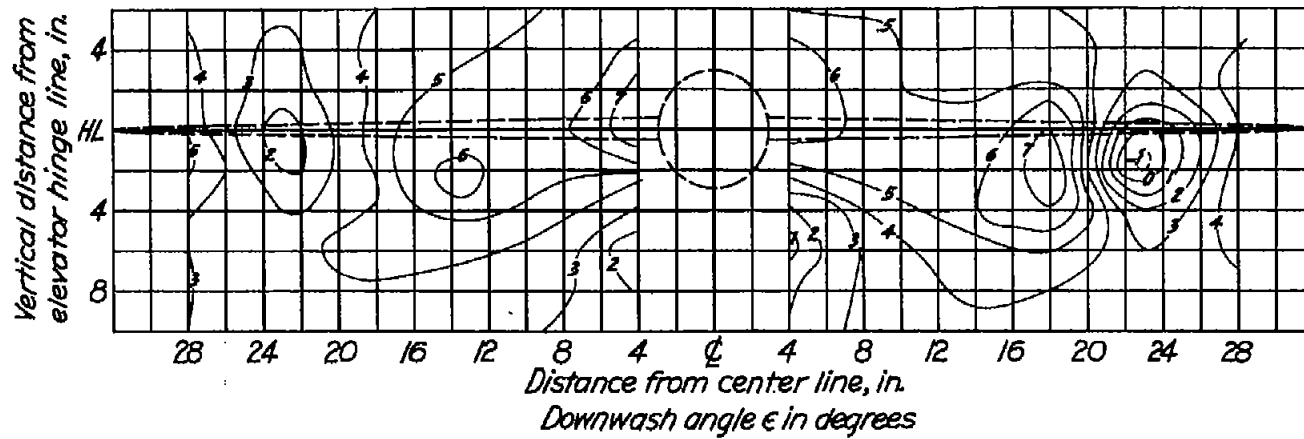
$$(a) \alpha_w = 0.2^\circ.$$

Figure 10.- Downwash angles and dynamic-pressure ratios in the vertical plane of the elevator hinge line. View looking upstream.  $\delta_f = 0^\circ$ ;  $T_c = 0$ ;  $R \approx 2,440,000$ .



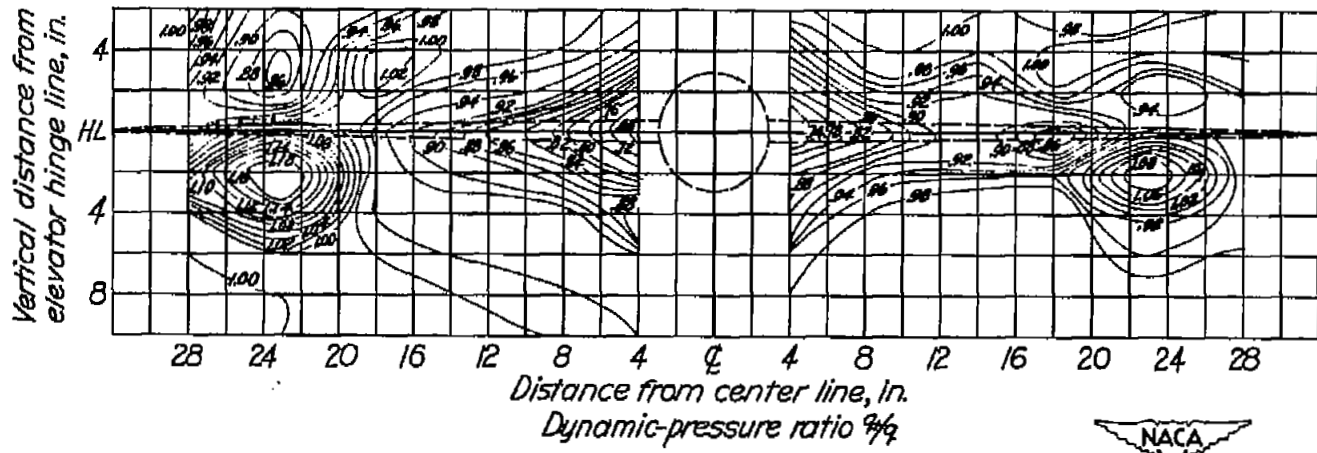
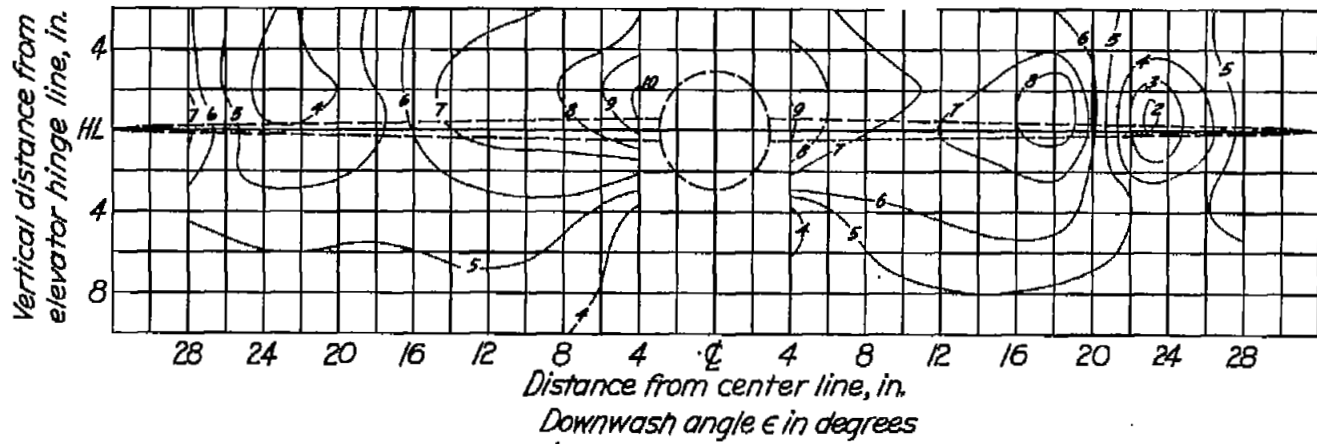
(b)  $\alpha_w = 3.4^\circ$ .

Figure 10.- Continued.



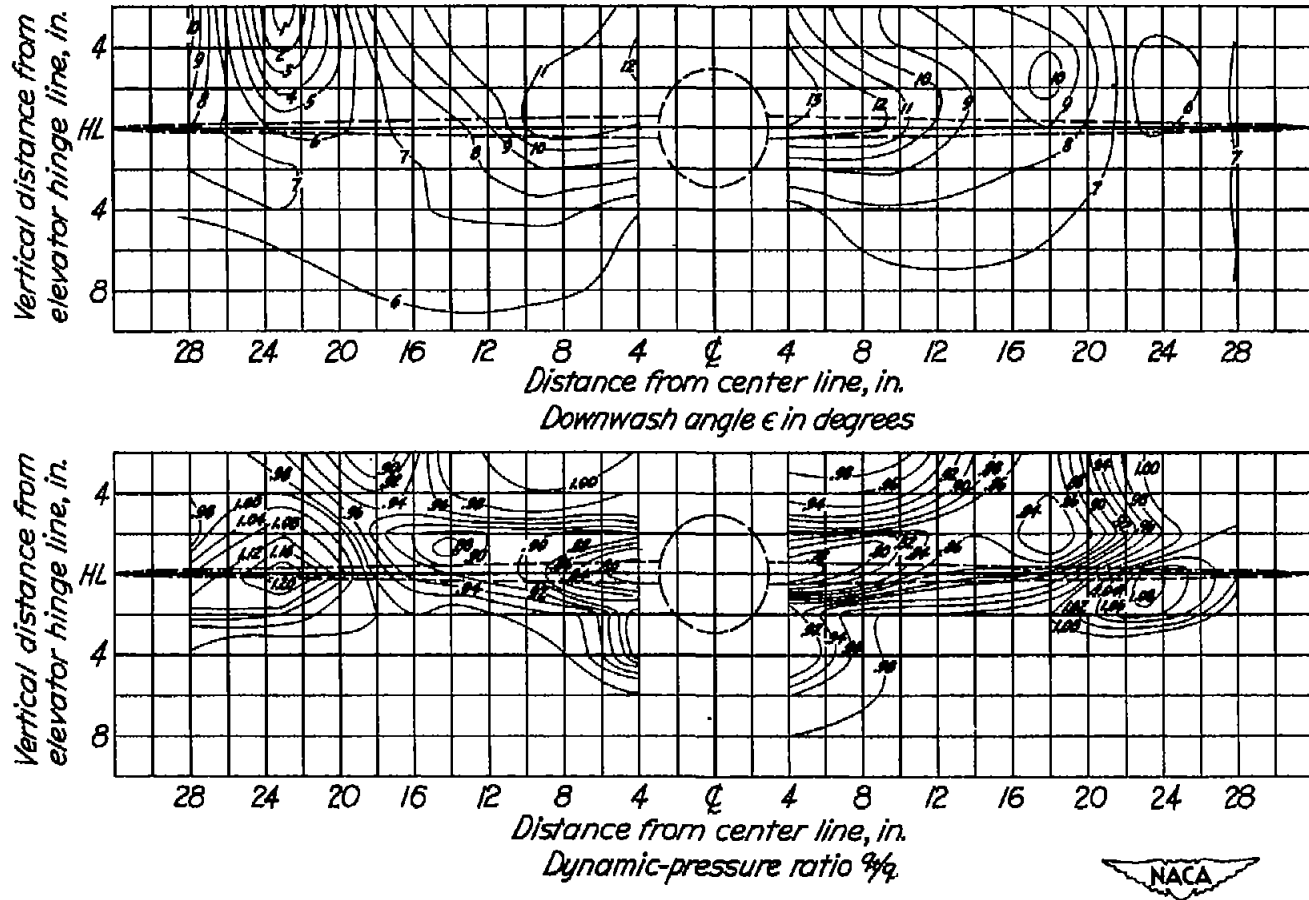
(c)  $\alpha_w = 7.7^\circ$ .

Figure 10.- Continued.



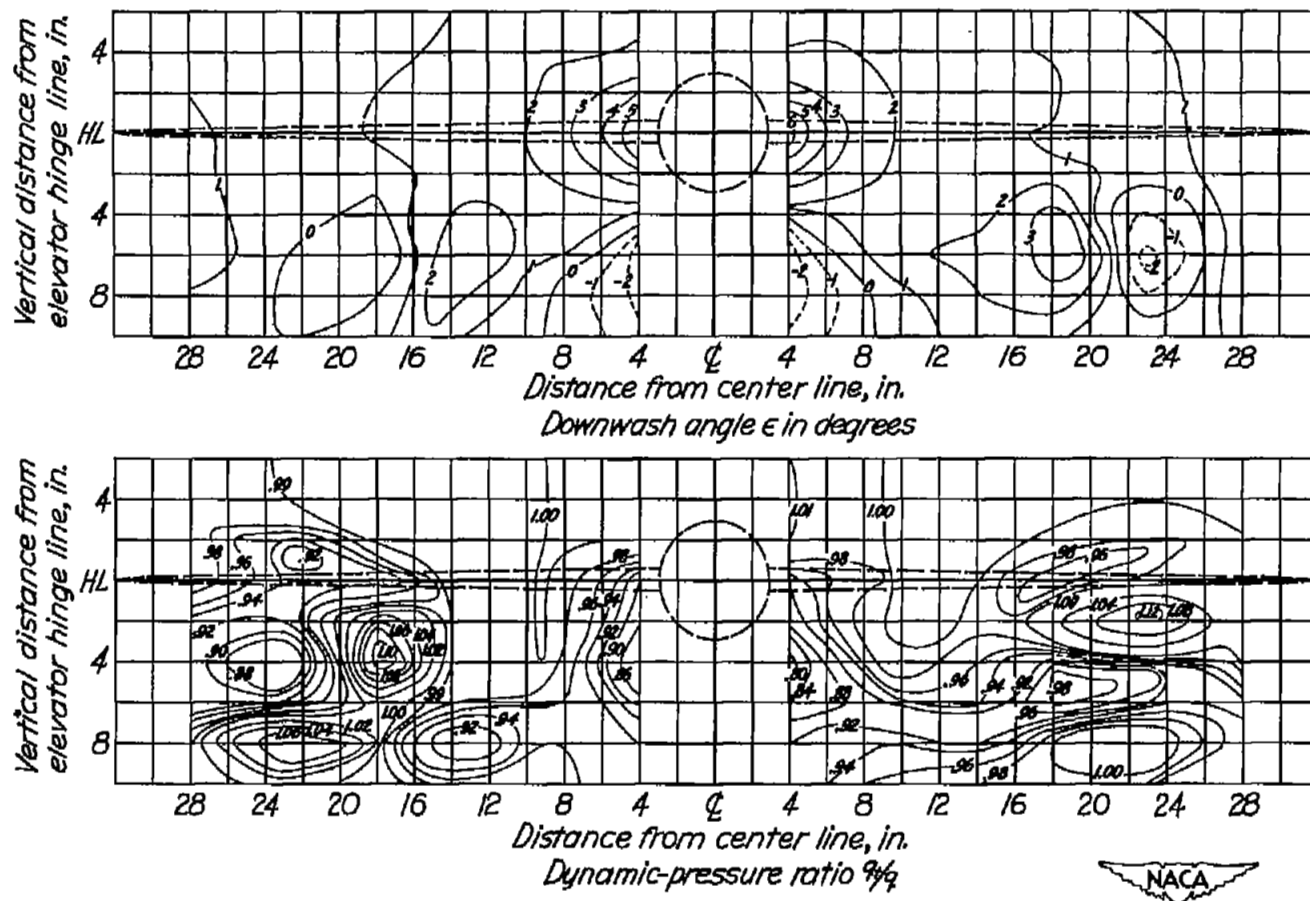
(d)  $\alpha_w = 11.9^\circ$ .

Figure 10.- Continued.



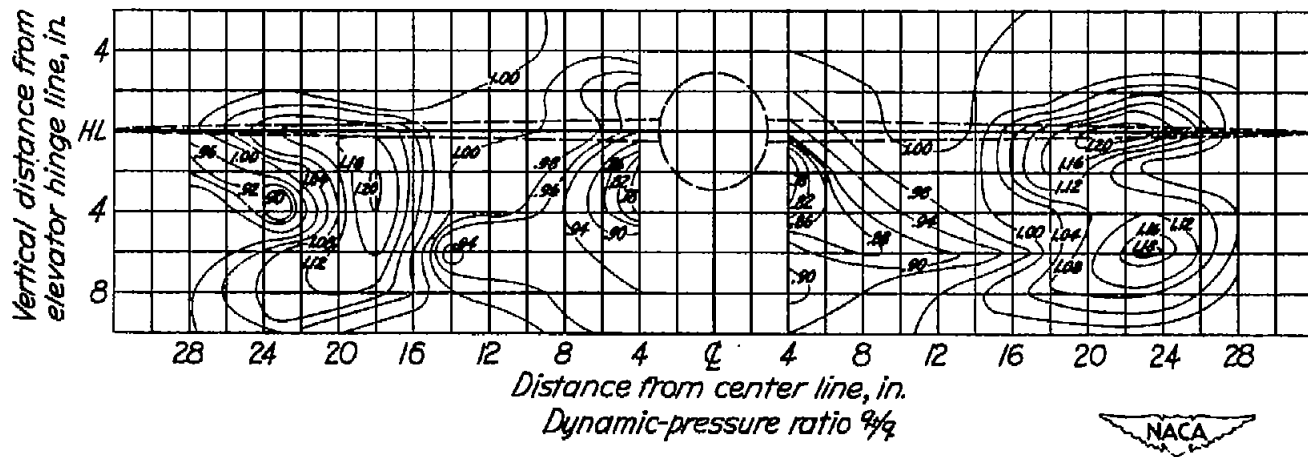
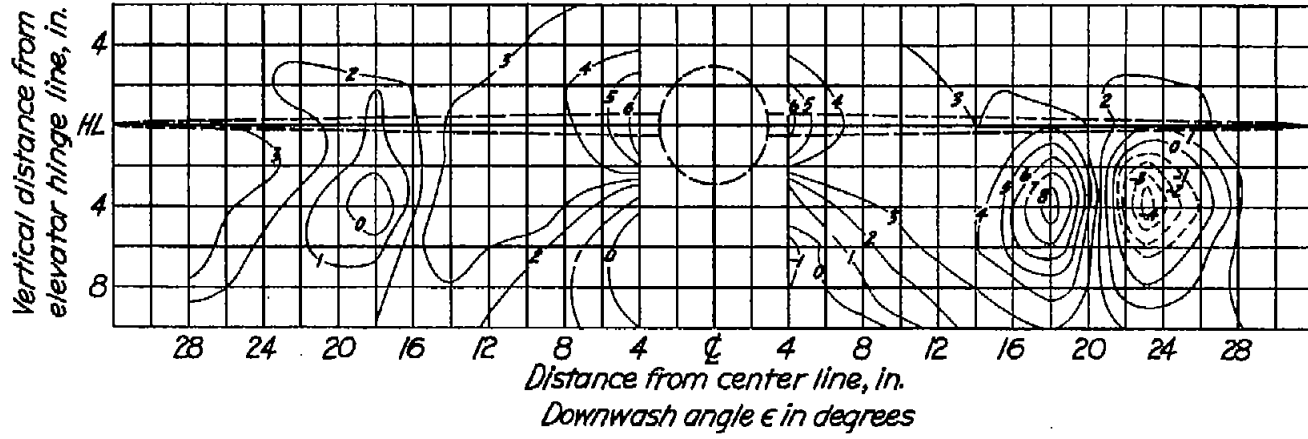
$$(e) \alpha_w = 16.1^\circ$$

Figure 10.- Concluded.



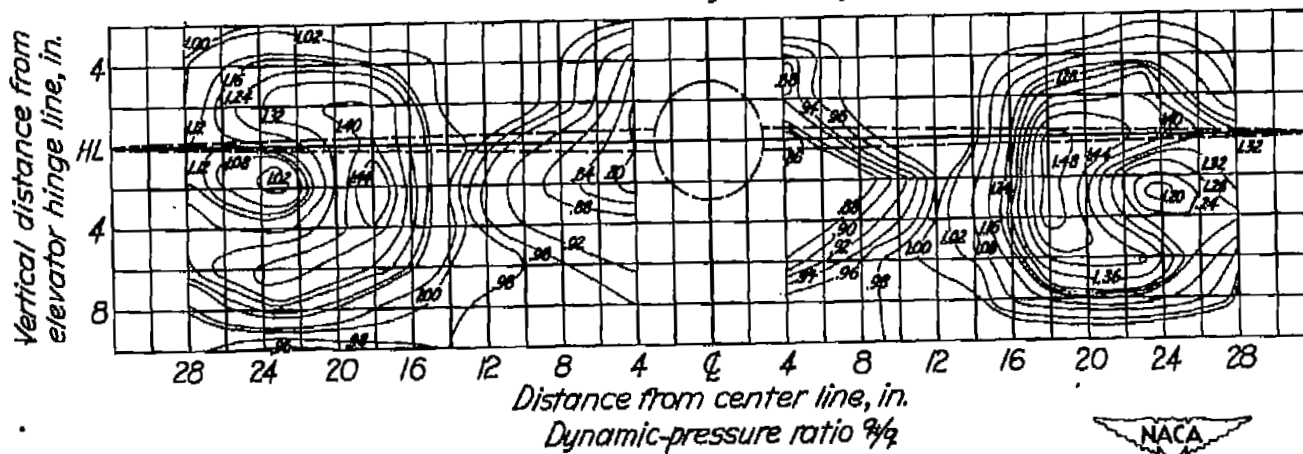
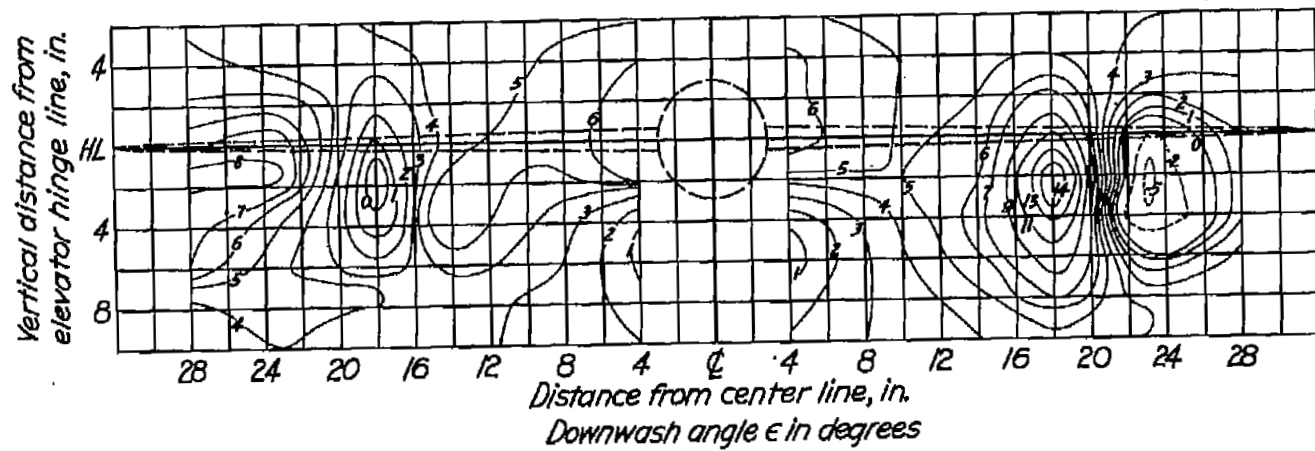
(a)  $\alpha_w = 0.2^\circ$ .

Figure 11.- Downwash angles and dynamic-pressure ratios in the vertical plane of the elevator hinge line. View looking upstream.  $\delta_f = 0^\circ$ ; 100-percent rated power;  $R \approx 2,440,000$ .



(b)  $\alpha_{PV} = 3.4^\circ$ .

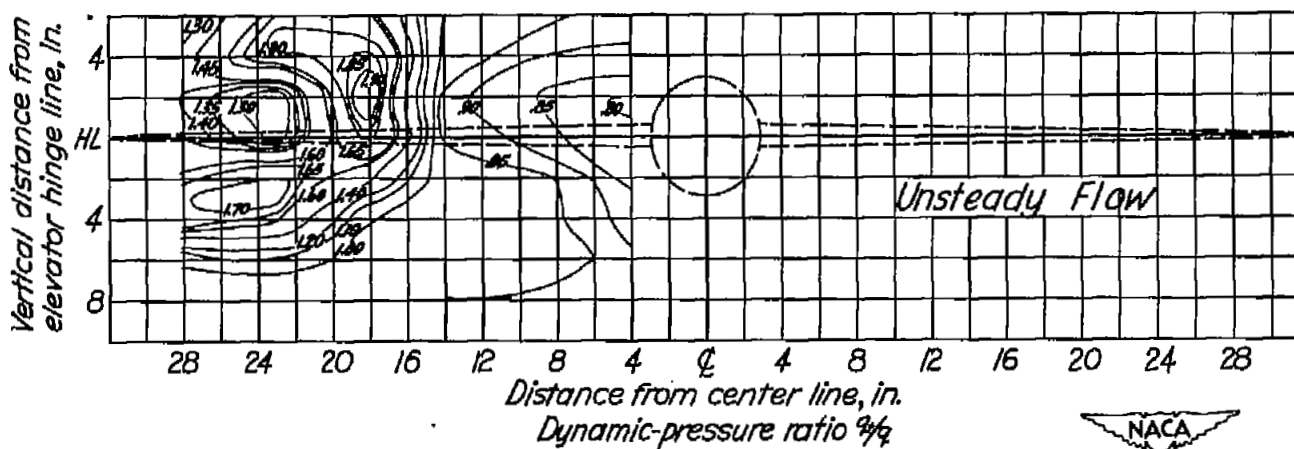
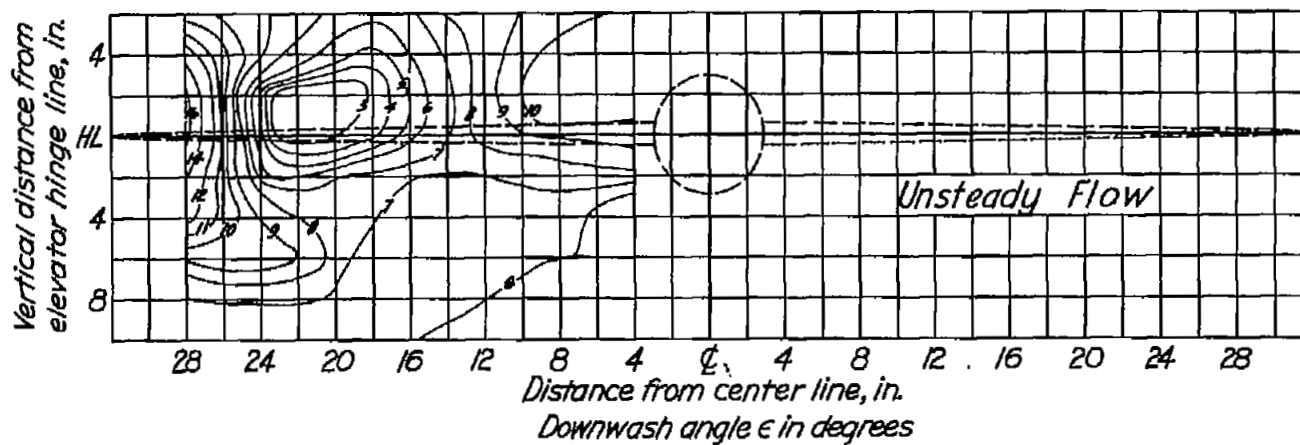
Figure 11.- Continued.



(c)  $\alpha_w = 7.8^\circ$ .

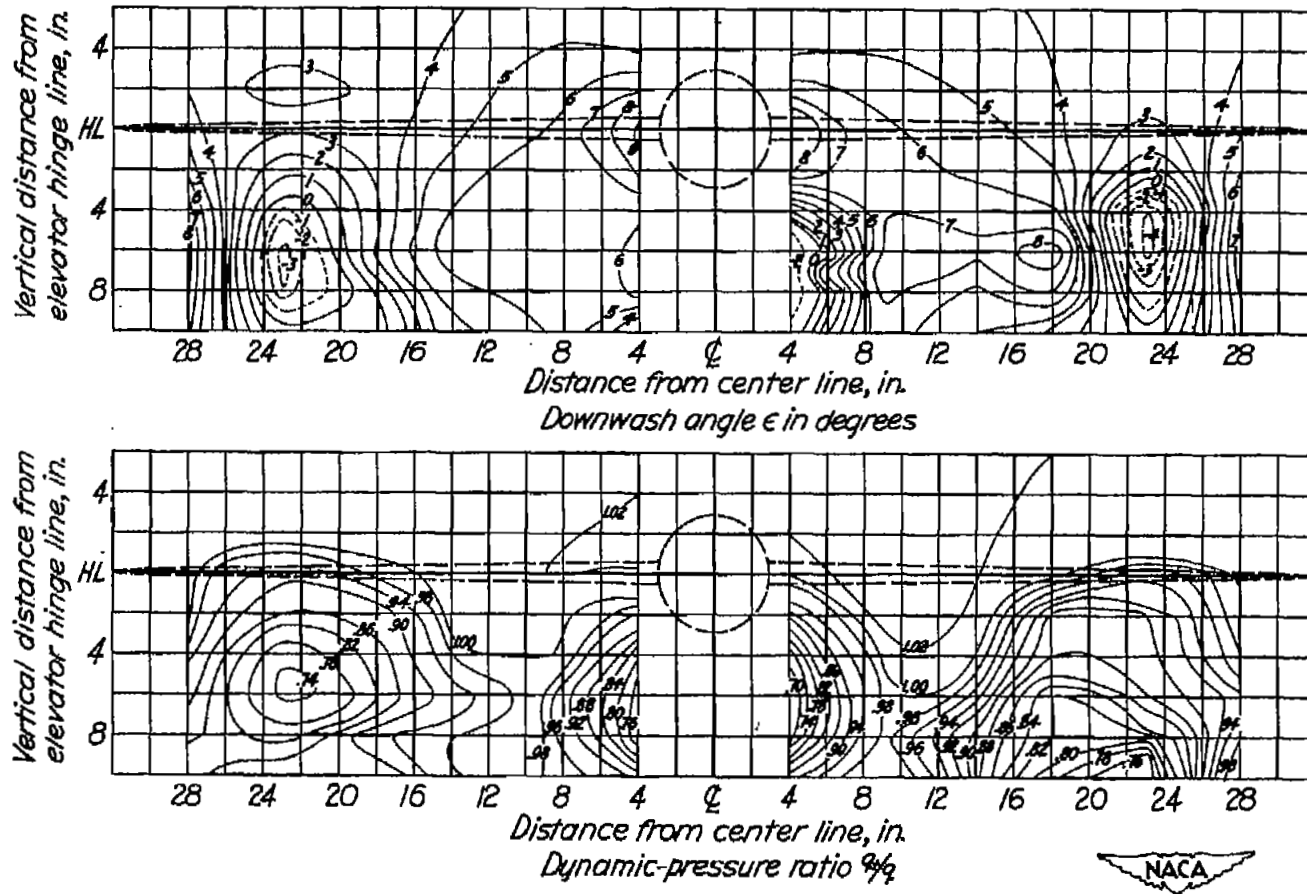
Figure 11.- Continued.





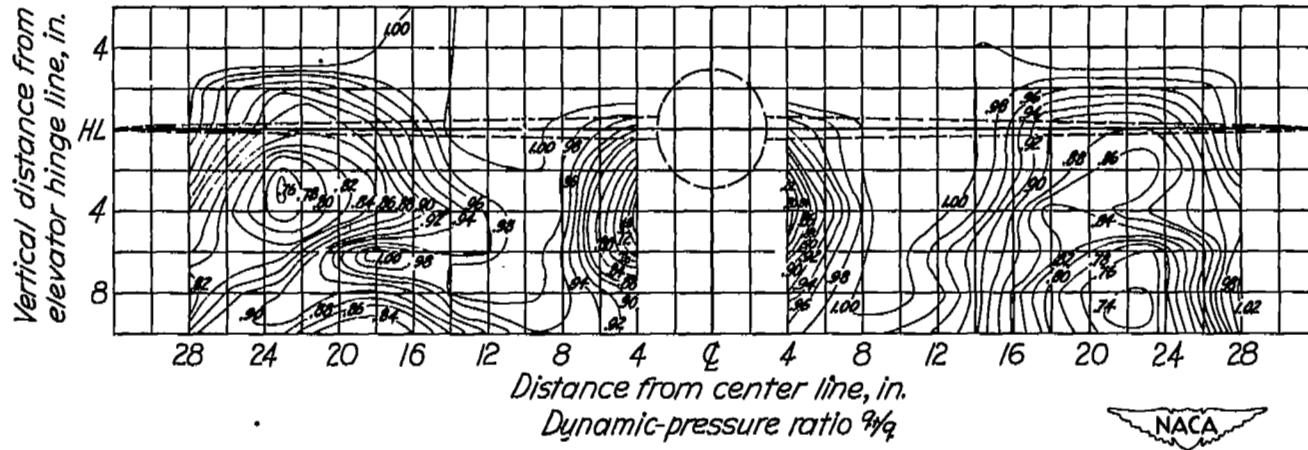
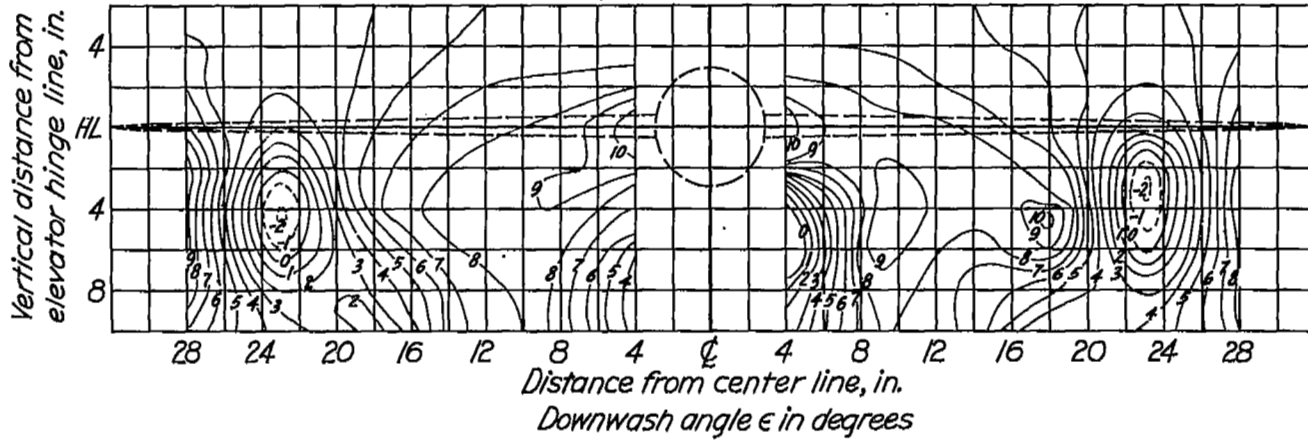
(e)  $\alpha_w = 16.2^\circ$ .

Figure 11.- Concluded.



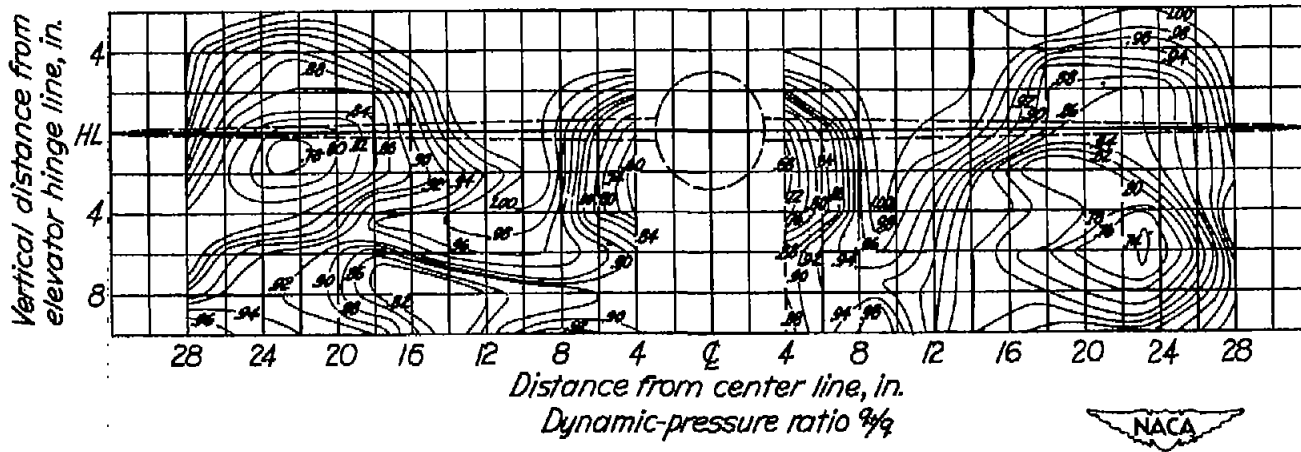
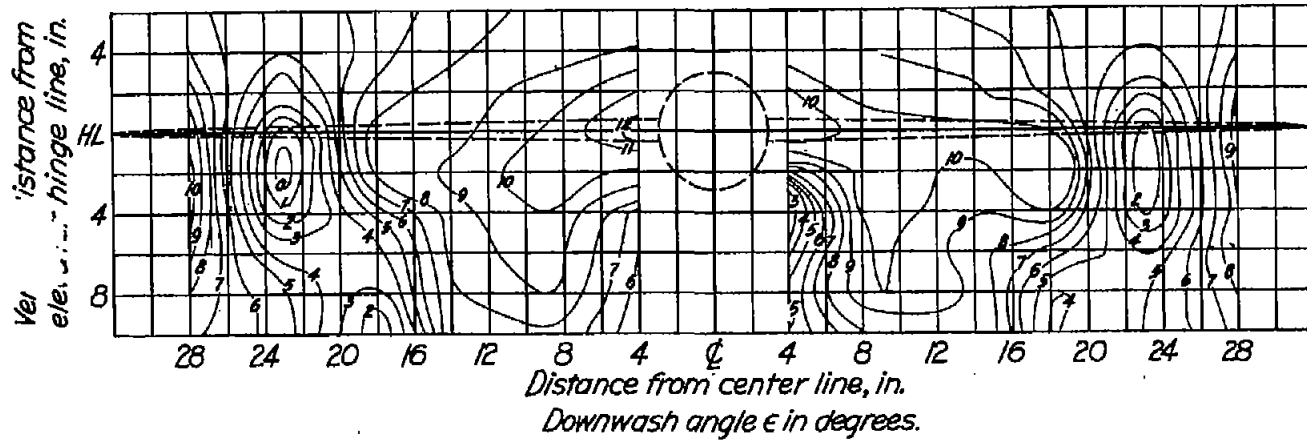
(a)  $\alpha_w = 0.5^\circ$ .

Figure 12.- Downwash angles and dynamic-pressure ratios in the vertical plane of the elevator hinge line. View looking upstream.  $\delta_f = 20^\circ$ ;  $T_c = 0$ ;  $R \approx 2,440,000$ .



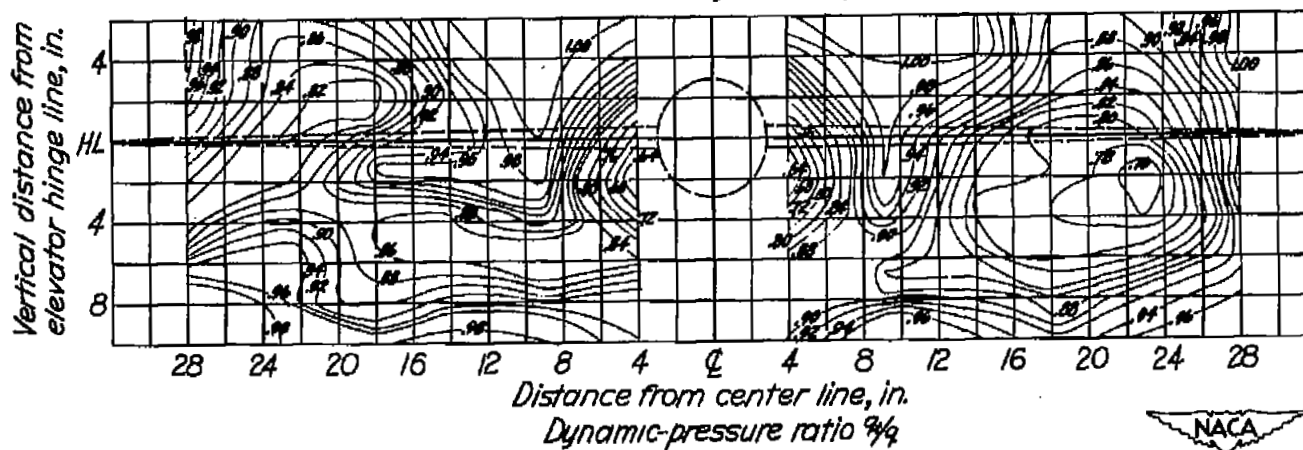
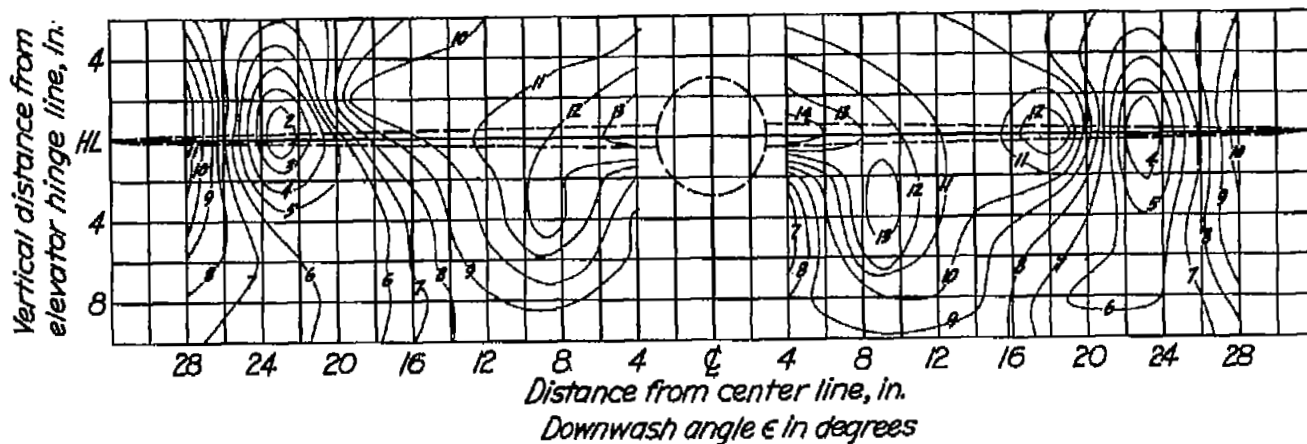
(b)  $\alpha_w = 4.7^\circ$ .

Figure 12.- Continued.



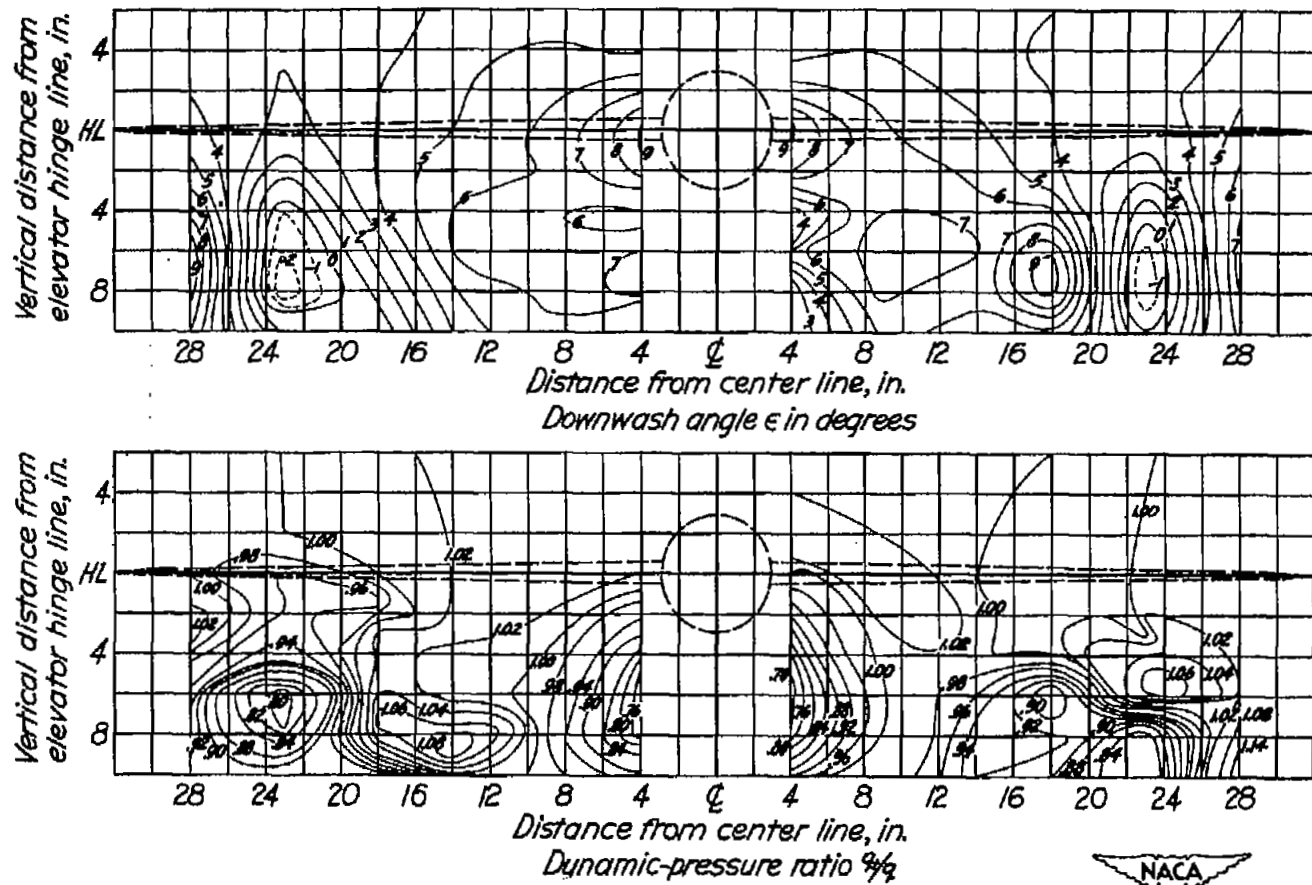
$$(c) \alpha_w = 9.0^\circ$$

Figure 12.- Continued.



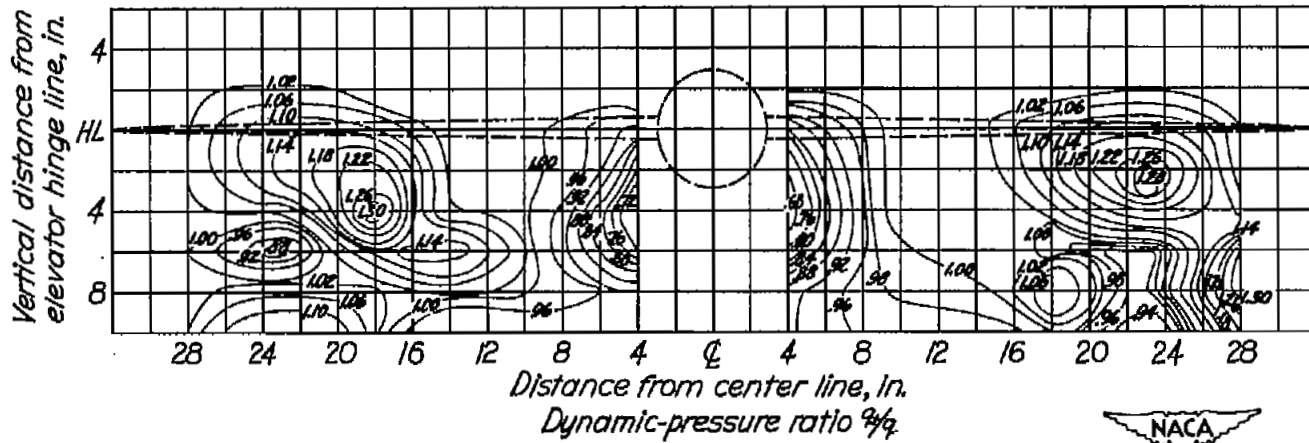
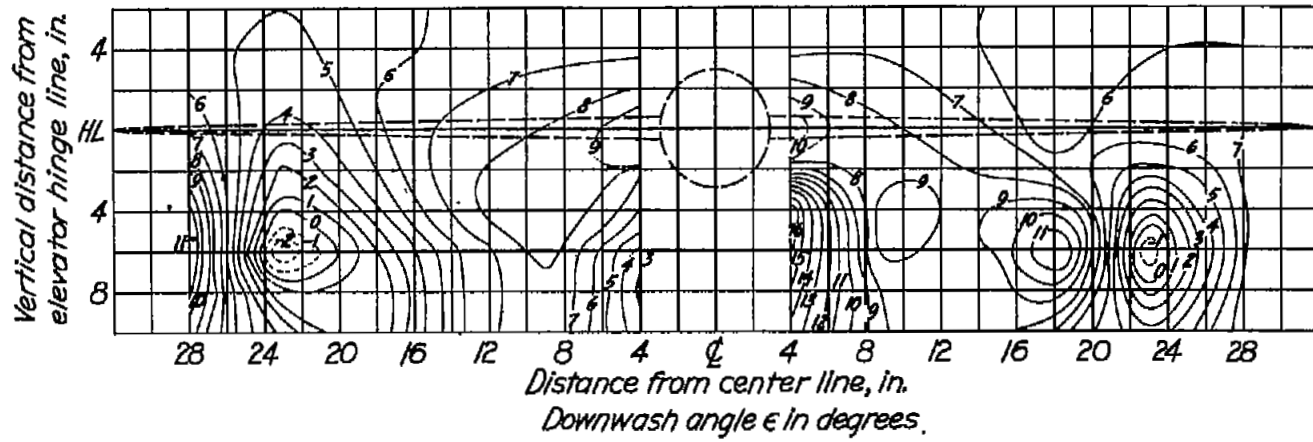
(d)  $\alpha_w = 13.2^\circ$ .

Figure 12.- Concluded.



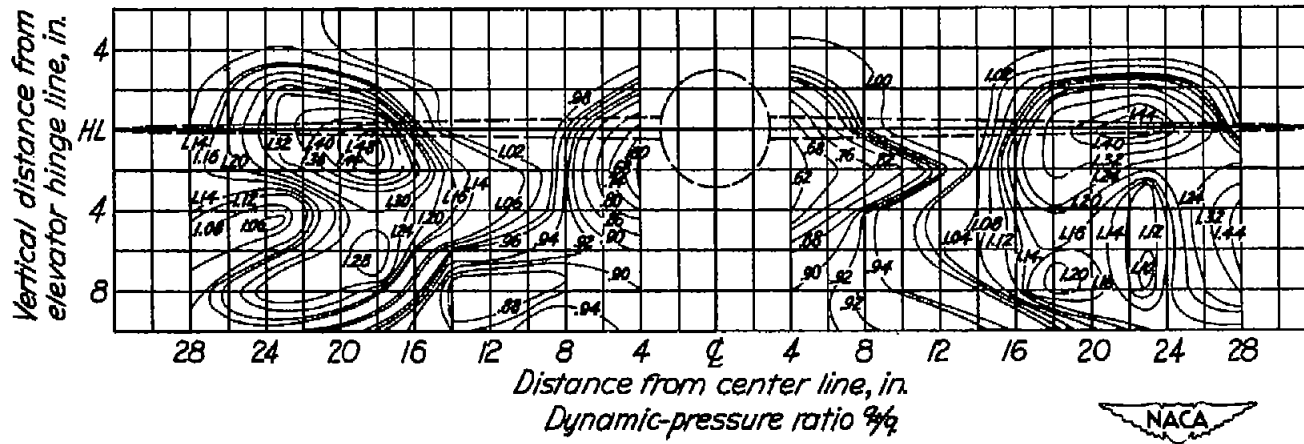
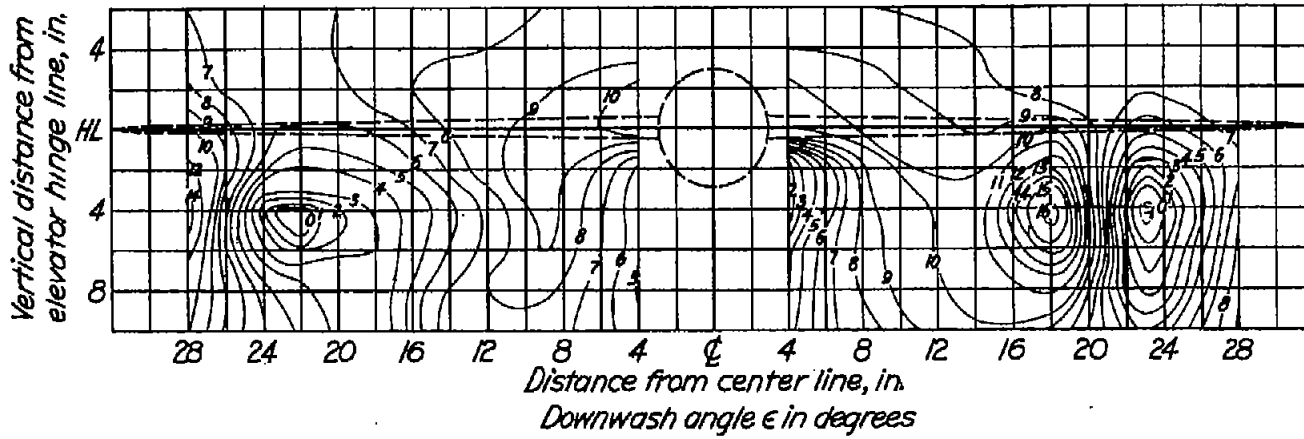
$$(a) \alpha_w = 0.5^\circ.$$

Figure 13.- Downwash angles and dynamic-pressure ratios in the vertical plane of the elevator hinge line. View looking upstream.  $\delta_f = 20^\circ$ ; 75-percent rated power;  $R \approx 2,440,000$ .



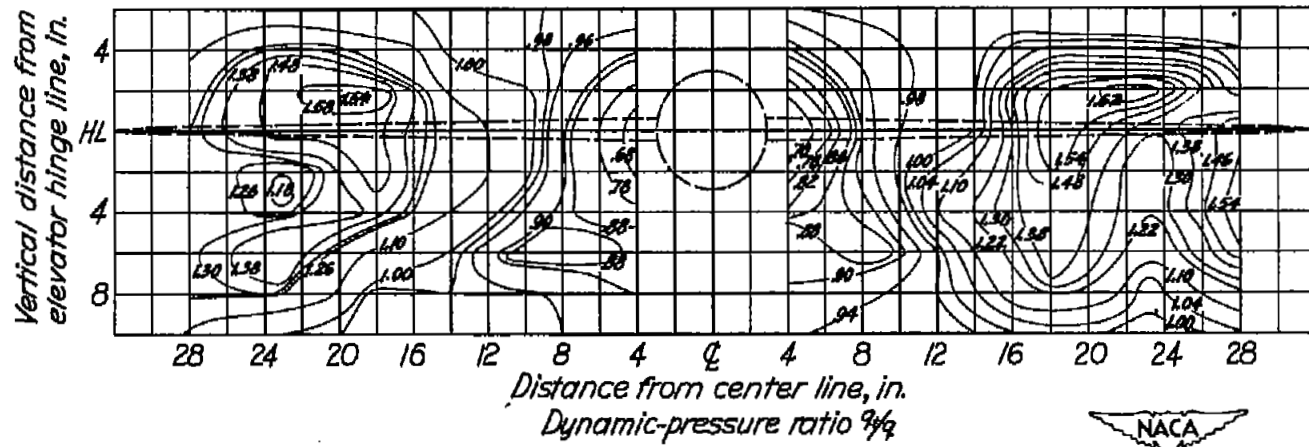
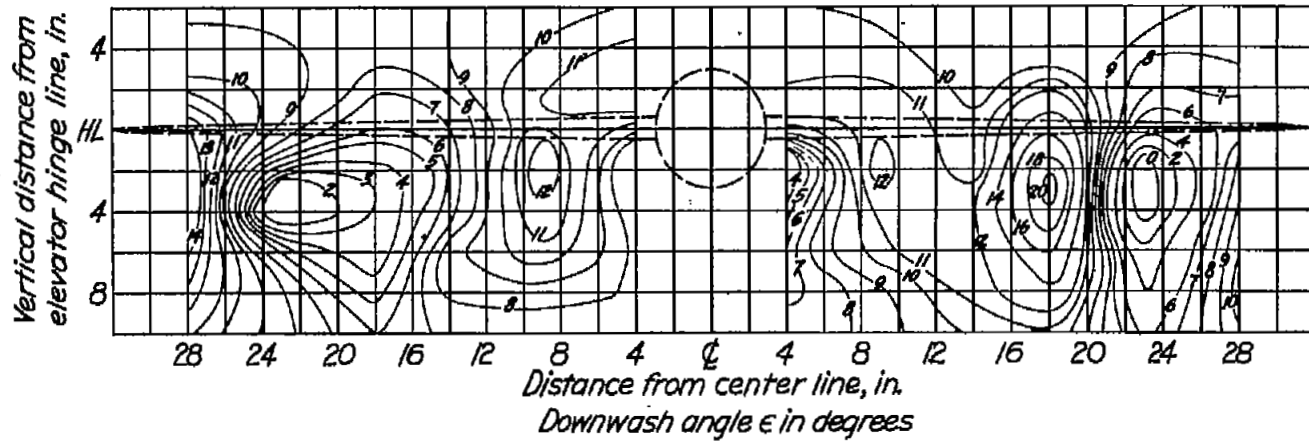
(b)  $\alpha_w = 4.8^\circ$ .

Figure 13.- Continued.



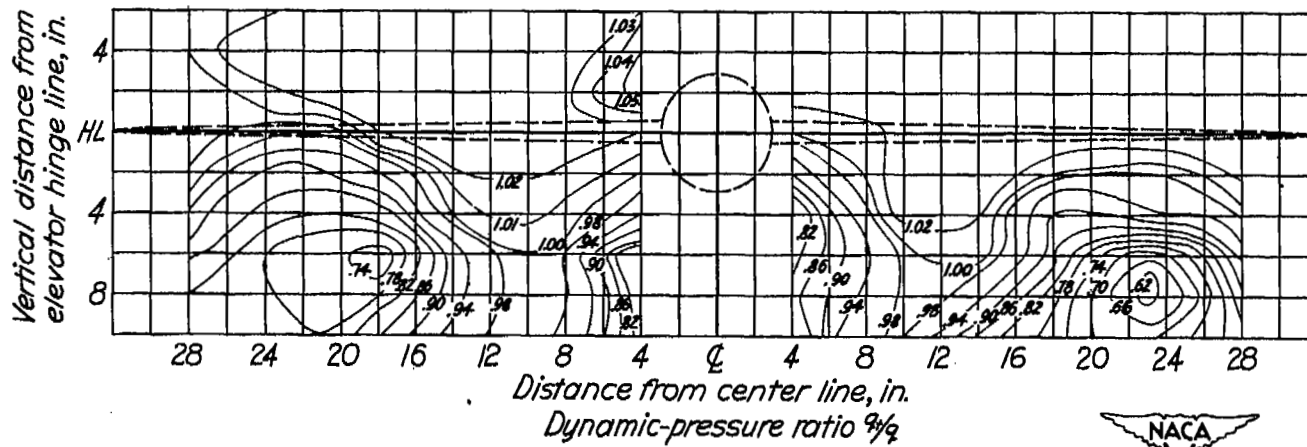
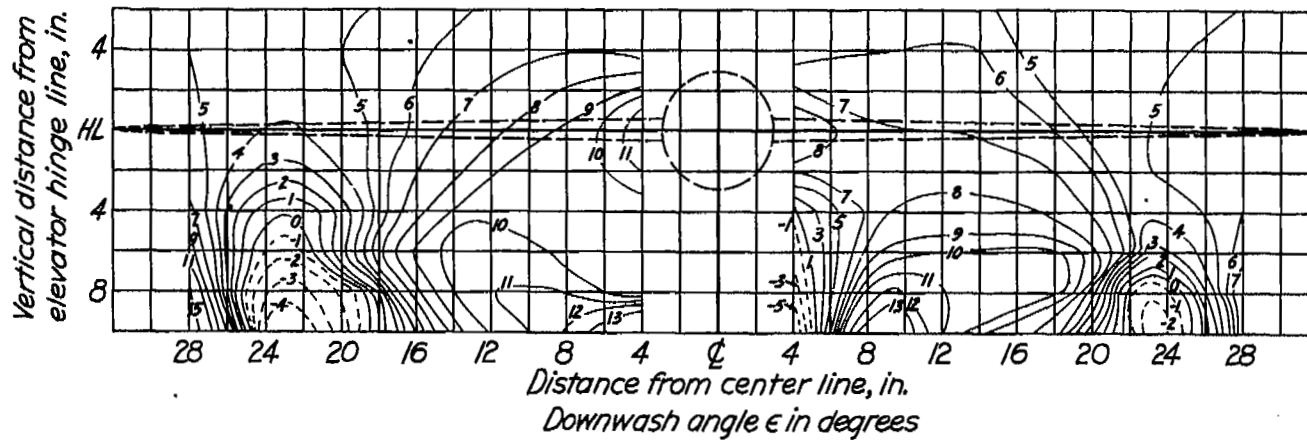
$$(c) \alpha_w = 9.1^\circ$$

Figure 13.- Continued.



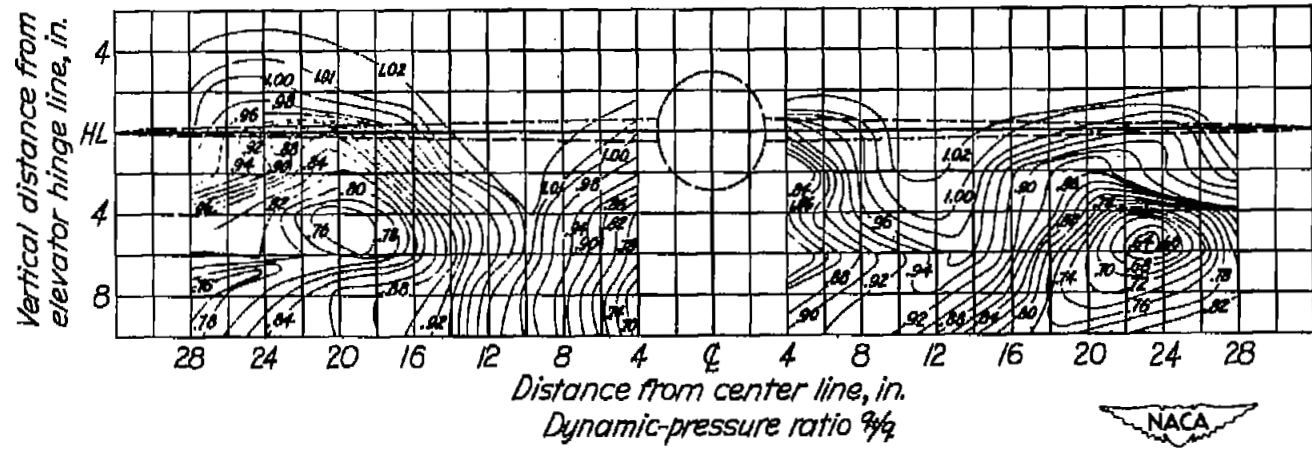
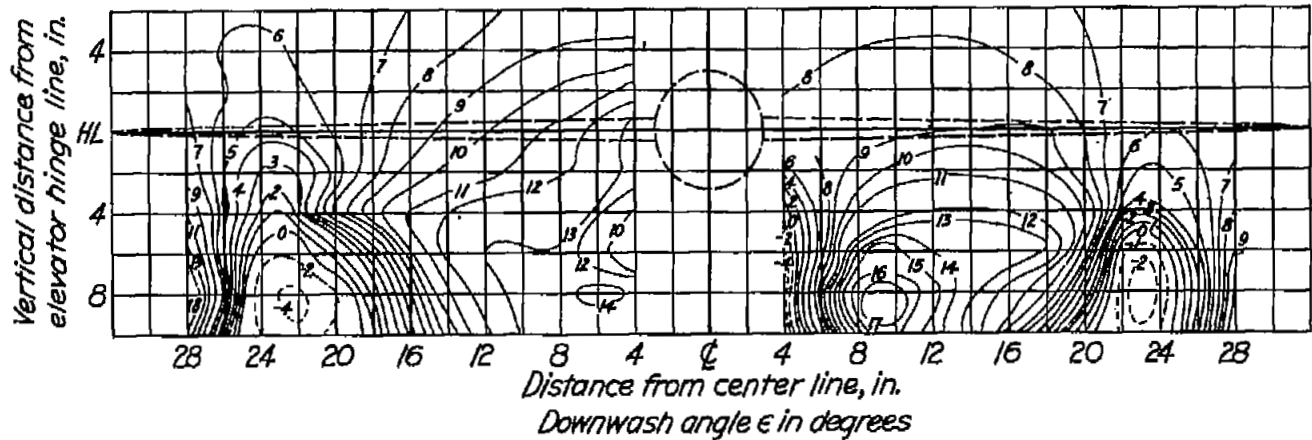
(d)  $\alpha_w = 13.4^\circ$ .

Figure 13.- Concluded.



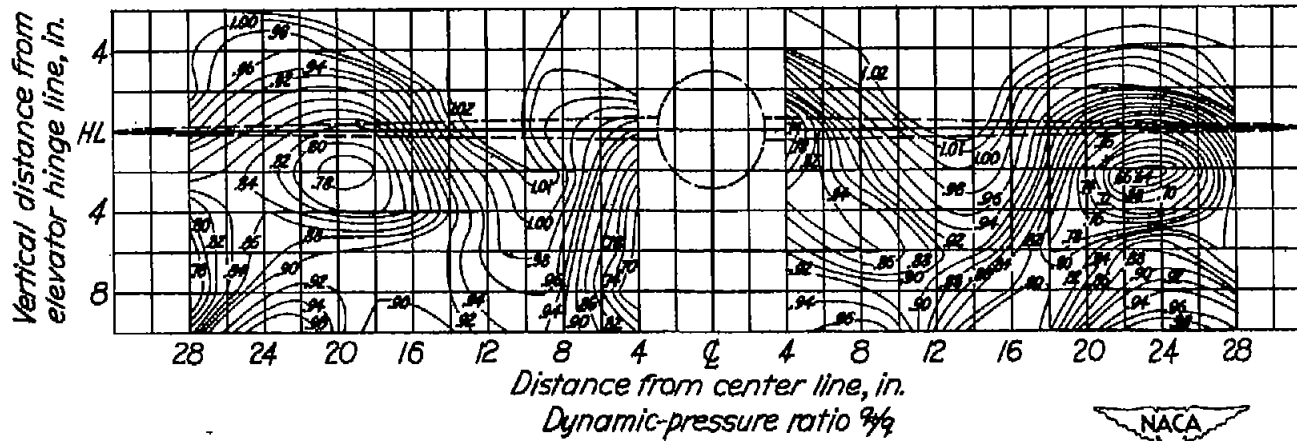
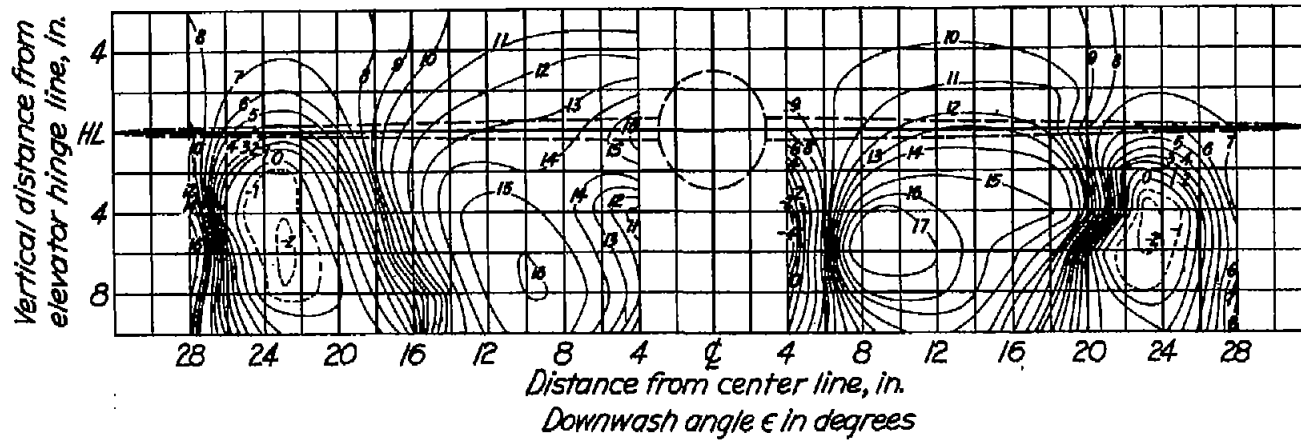
(a)  $\alpha_w = 0.7^\circ$ .

Figure 14.- Downwash angles and dynamic-pressure ratios in the vertical plane of the elevator hinge line. View looking upstream.  $\delta_f = 40^\circ$ ;  $T_c = 0$ ;  $R \approx 2,440,000$ .



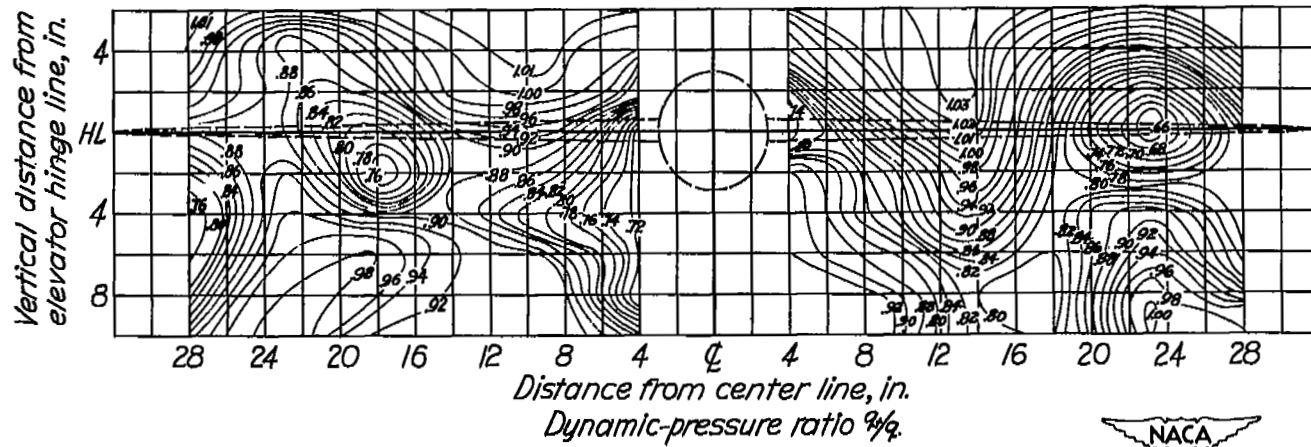
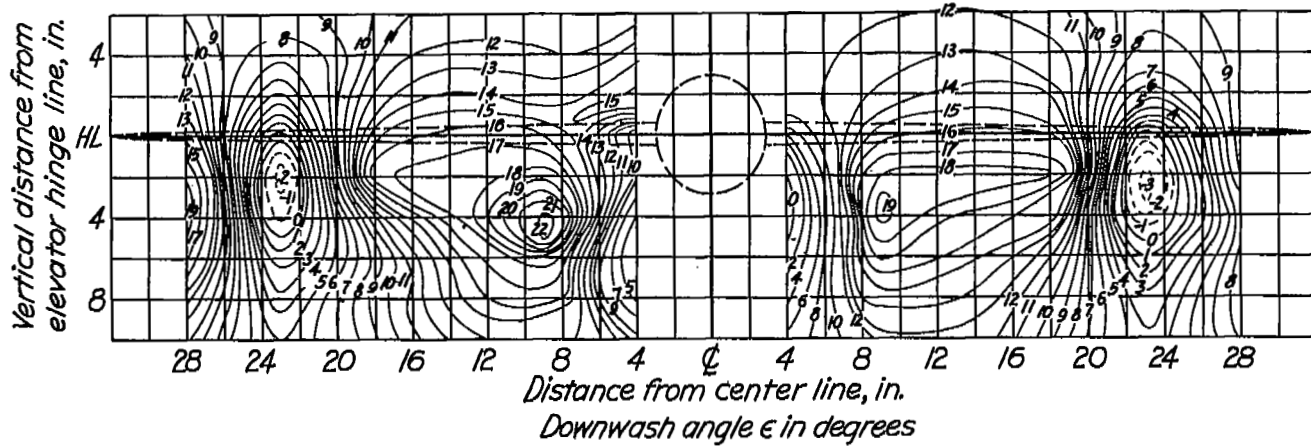
(b)  $\alpha_w = 5.0^\circ$ .

Figure 14.- Continued.



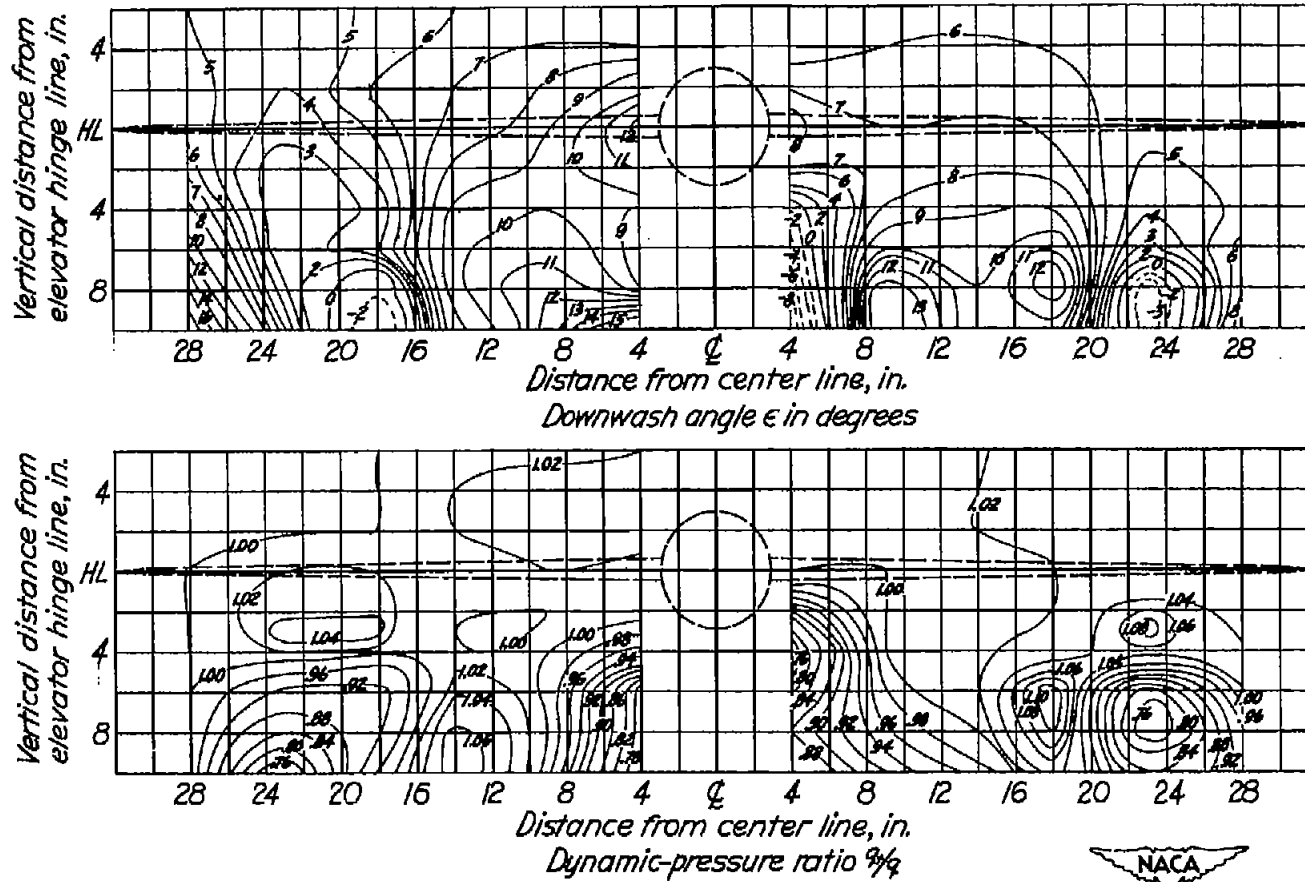
$$(c) \alpha_w = 9.2^\circ.$$

Figure 14.- Continued.



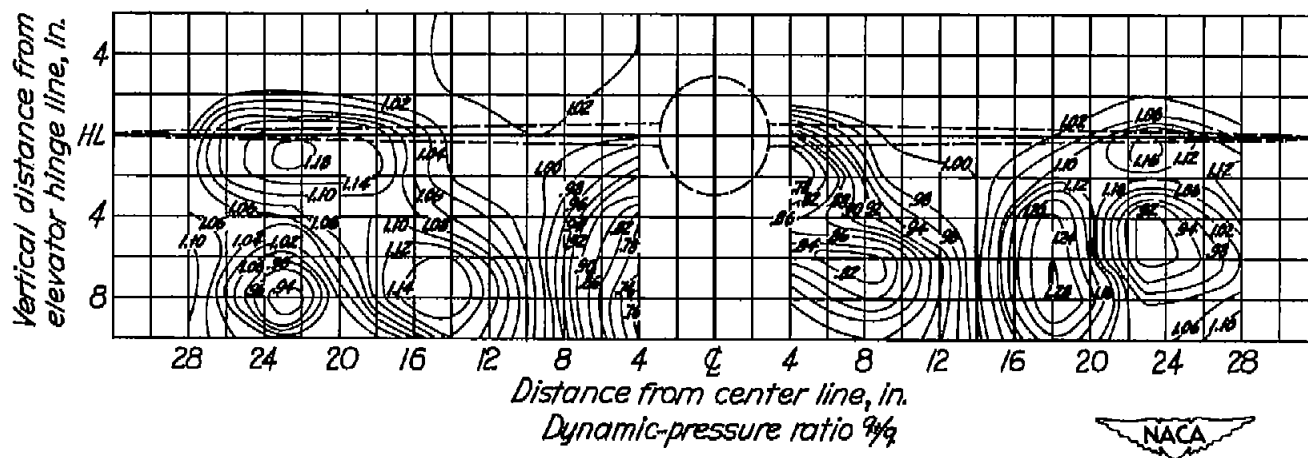
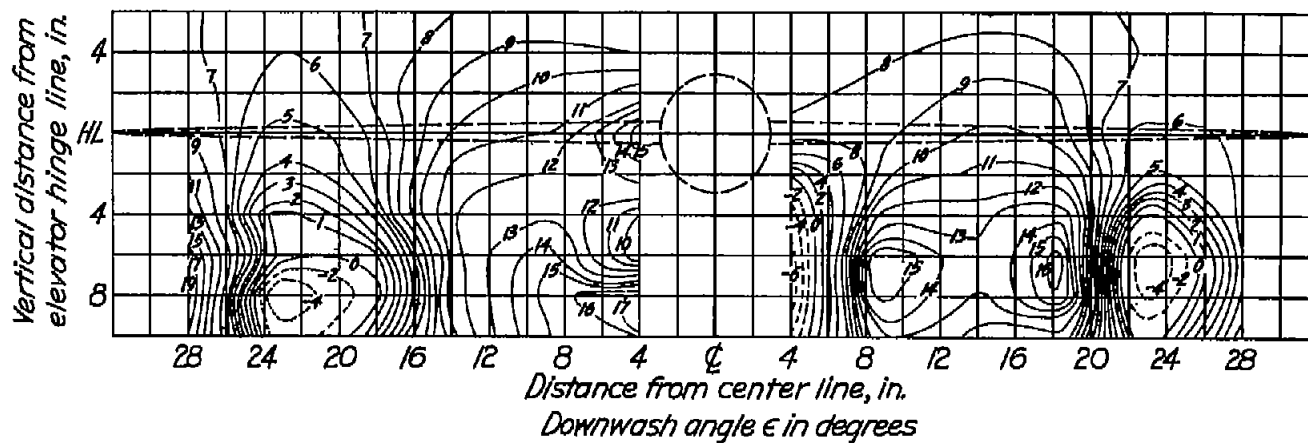
(d)  $\alpha_w = 13.5^\circ$ .

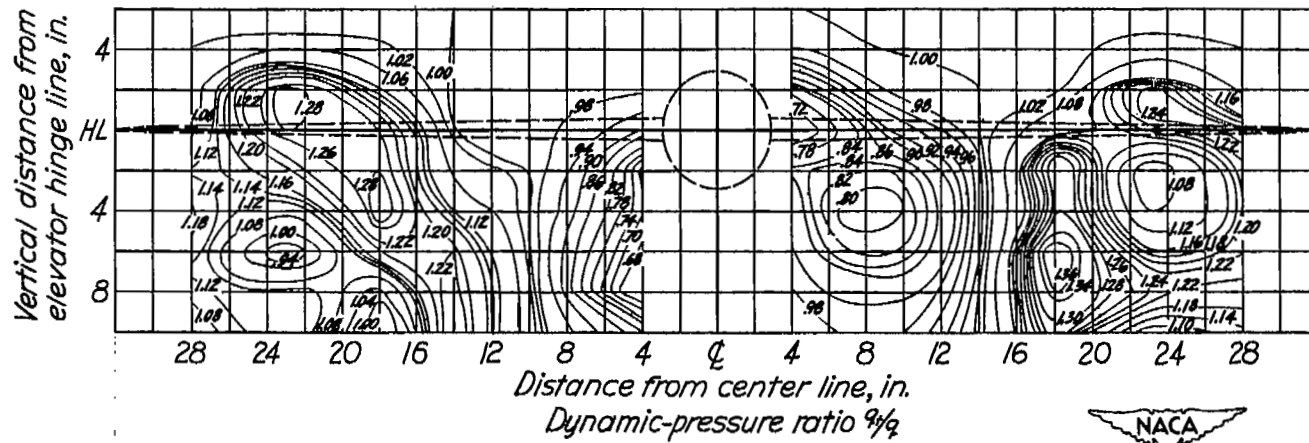
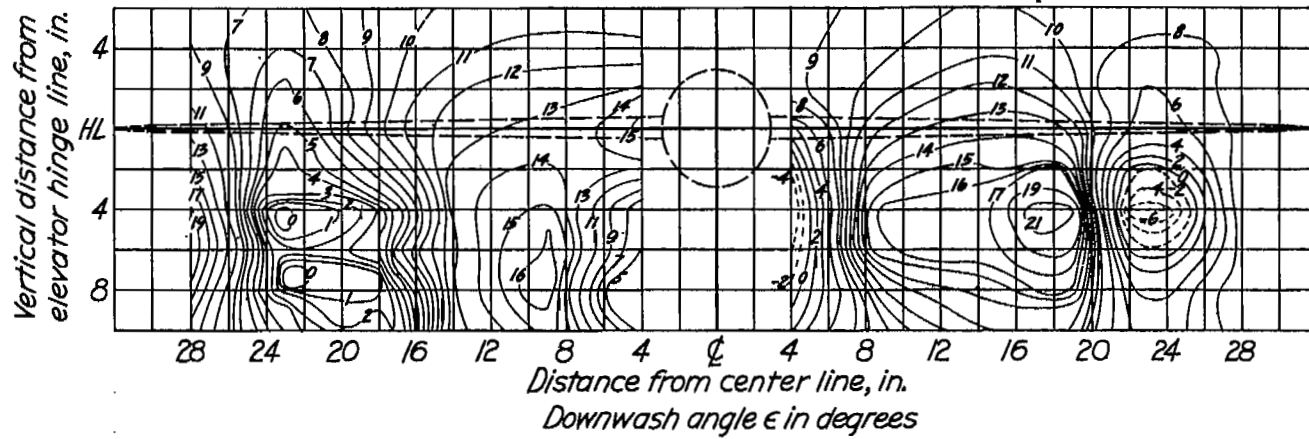
Figure 14.- Concluded.



(a)  $\alpha_w = 0.7^\circ$ .

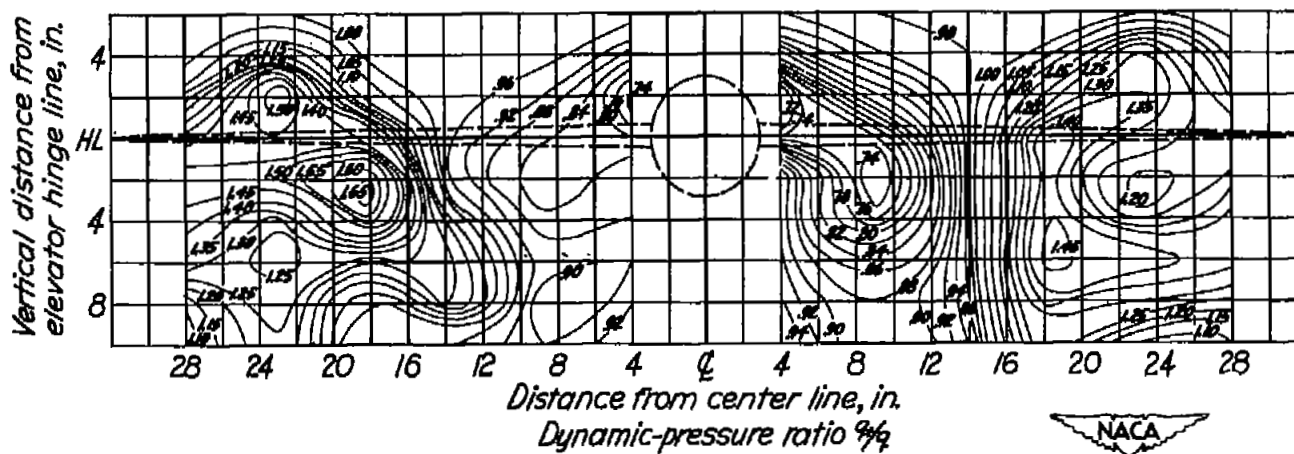
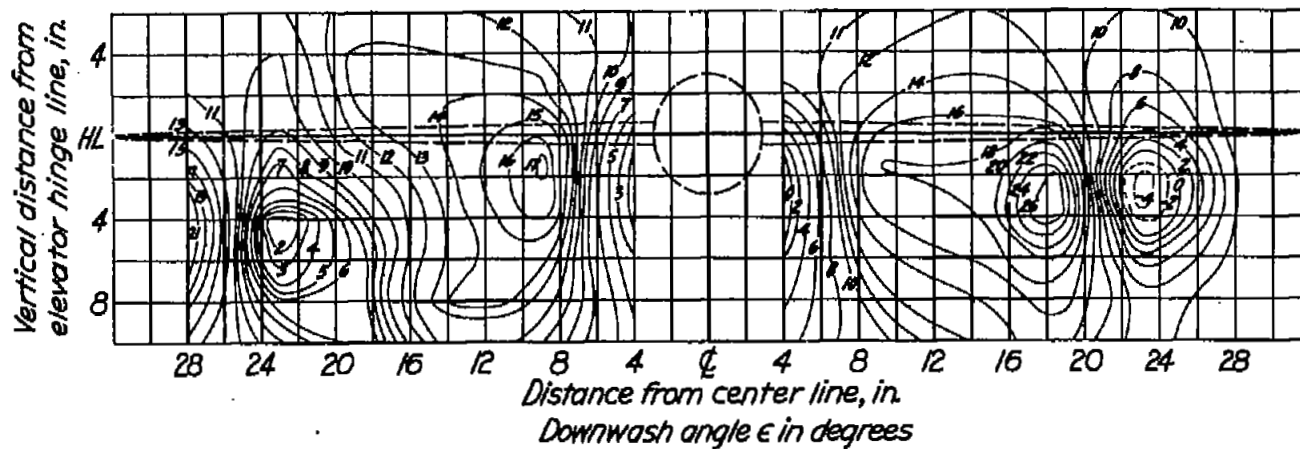
Figure 15.- Downwash angles and dynamic-pressure ratios in the vertical plane of the elevator hinge line. View looking upstream.  $\delta_f = 40^\circ$ ; 50-percent rated power;  $R \approx 2,440,000$ .





$$(c) \alpha_w = 9.3^\circ.$$

Figure 15.- Continued.



(d)  $\alpha_w = 13.6^\circ$ .

Figure 15.- Concluded.

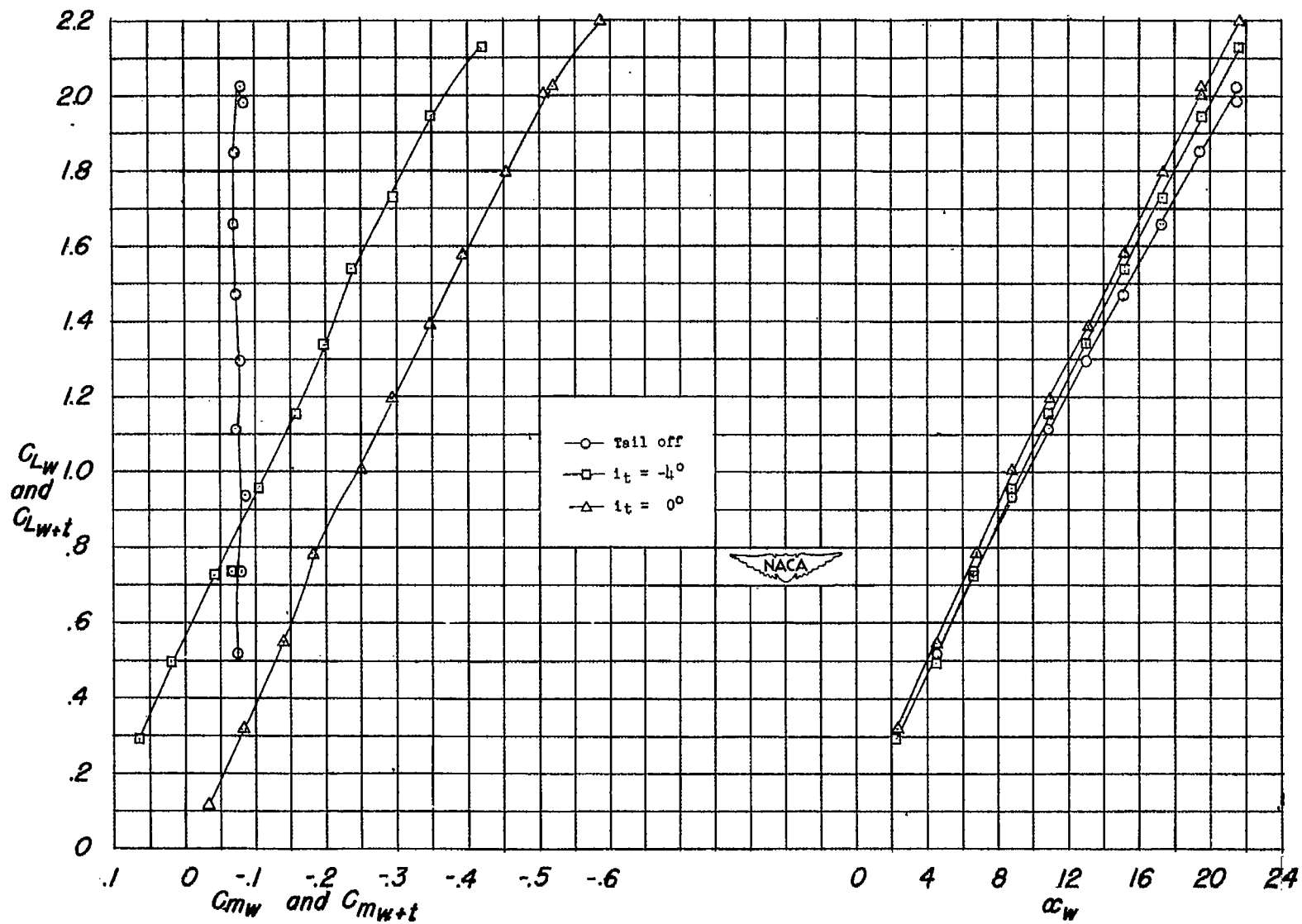
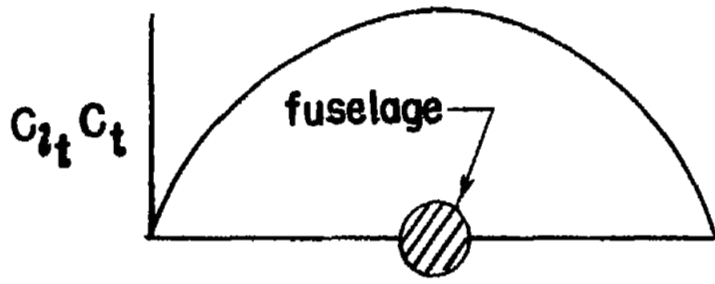
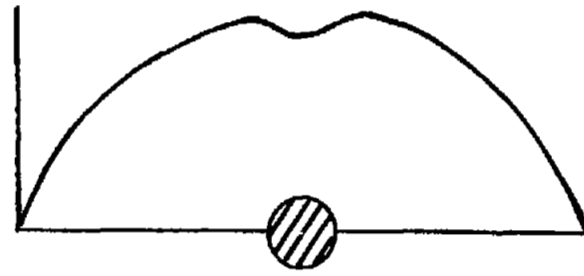


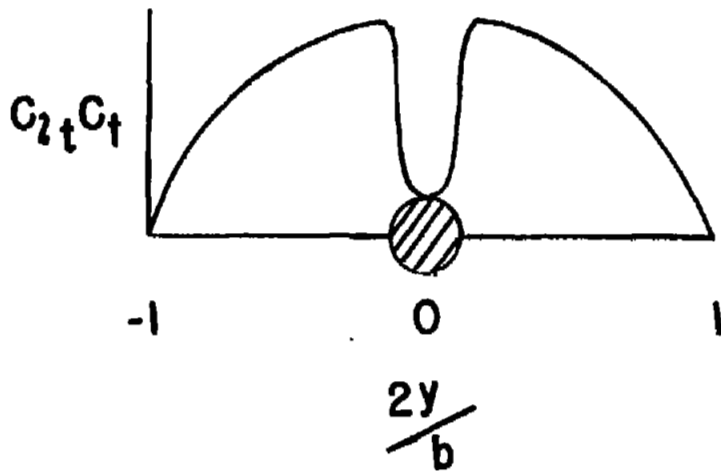
Figure 16.- Representative force and moment data.  $\delta_f = 0^\circ$ ; rated power.



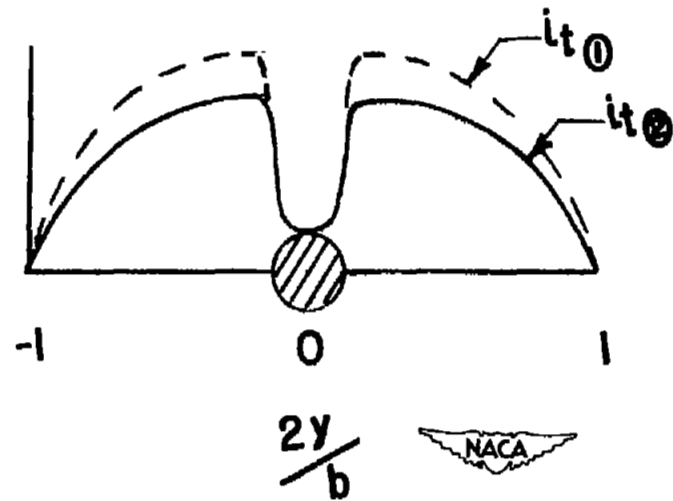
(a) Carry-over load.



(b) Theoretical load.



(c) Large fuselage boundary-layer and separation effects.



(d) Load of (c) for two values of  $i_t$ .

Figure 17.- Schematic loading over a tail-fuselage combination.